

# Learning Counterfactually Invariant Predictors

Francesco Quinzan<sup>\*1</sup>, Cecilia Casolo<sup>2</sup>, Krikamol Muandet<sup>3</sup>, Niki Kilbertus<sup>2,4</sup>, Yucen Luo<sup>3</sup>

<sup>1</sup>KTH Royal Institute of Technology

<sup>2</sup>Helmholtz AI, Munich

<sup>3</sup>Max Planck Institute for Intelligent Systems

<sup>4</sup>Technical University of Munich

*\*Part of this work was done while visiting the Max Planck Institute for Intelligent Systems.*

## Abstract

We propose a method to learn predictors that are invariant under counterfactual changes of certain covariates. This method is useful when the prediction target is causally influenced by covariates that should not affect the predictor output. For instance, an object recognition model may be influenced by position, orientation, or scale of the object itself. We address the problem of training predictors that are explicitly *counterfactually invariant* to changes of such covariates. We propose a model-agnostic regularization term based on conditional kernel mean embeddings, to enforce counterfactual invariance during training. We prove the soundness of our method, which can handle mixed categorical and continuous multi-variate attributes. Empirical results on synthetic and real-world data demonstrate the efficacy of our method in a variety of settings.

## 1 Introduction and related work

Invariance, or equivariance to certain transformations of data, has proven essential in numerous applications of machine learning (ML). Invariance leads to better generalization capabilities of ML models [Arjovsky et al., 2019, Bloem-Reddy and Teh, 2020, Chen et al., 2020]. For instance, in image recognition tasks, predictions ought to remain unchanged under scaling, translation, or rotation of the input image. Data augmentation is one of the earliest heuristics developed to promote this kind of invariance that has become indispensable in training successful models, like deep neural networks (DNNs) [Shorten and Khoshgoftaar, 2019, Xie et al., 2020]. State-of-the-art architectures can handle invariance and equivariance requirements by design. Well-known examples include convolutional neural networks (CNNs) for translation invariance of image data [Krizhevsky et al., 2012], group equivariant CNNs for other group transformations [Cohen and Welling, 2016], recurrent neural networks (RNNs) and transformers for sequential data [Vaswani et al., 2017], DeepSet [Zaheer et al., 2017] for sets, and graph neural networks (GNNs) for different types of geometric structures [Battaglia et al., 2018].

Many real-world applications in modern ML, however, call for an arguably stronger notion of invariance, called *counterfactual invariance*. This is the case for image classification, algorithmic fairness [Hardt et al., 2016, Mitchell et al., 2021], robustness [Bühlmann, 2020], and out-of-distribution generalization [Lu et al., 2021]. These applications require predictors to exhibit invariance with respect to hypothetical manipulations of the data generating process (DGP) [Arjovsky et al., 2019, Bühlmann, 2020, Heinze-Deml et al., 2018, Peters et al., 2016, Rojas-Carulla et al., 2018]. In image classification, for instance, we want to build a model that “would have made the same prediction, if the object position had been different with everything else being equal”. This model ought to be invariant to the DGP of some attributes, such as an object position and light condition. Similarly, in algorithmic fairness Kilbertus et al. [2017], Kusner et al. [2017] introduce notions of interventional and counterfactual fairness. These

notions are based on the causal relationships between the observed variables of a model, and they require invariance to the DGP of protected attributes.

Inspired by problems in natural language processing (NLP), Veitch et al. [2021] study a notion of counterfactual invariance. In their work, Veitch et al. [2021] provide a method to enforce their notion of counterfactual invariance, based on the maximum mean discrepancy (MMD). However, this method promotes only a *necessary*, but not sufficient observable imprint or proxy of counterfactual invariance during training. Furthermore, their work can only handle discrete random variables, and it applies to specific causal graphs. Motivated by this line of research, we study the following question:

*How do we learn predictors that are invariant  
under counterfactual changes of certain covariates?*

We propose a new definition of counterfactual invariance that generalizes the notion studied by Veitch et al. [2021]. Furthermore, we propose a new method that directly enforces counterfactual invariance during the learning process. Unlike existing approaches, the proposed method is *sufficient* for counterfactual invariance, and it works well for both categorical and continuous covariates and outcomes, as well as in multivariate settings

**Technical overview.** Our notion of counterfactual invariance inevitably relies on strong assumptions about the DGP, as counterfactuals by their very nature cannot be observed. This is a major challenge, since counterfactual invariance cannot be checked, unless strong prior knowledge of the DGP is available. We circumvent this problem by deriving a connection between counterfactual invariance and conditional independence, under certain observability assumptions in the causal graph. The resulting conditional independence statements can then be enforced via a regularization term based on the flexible Hilbert-Schmidt Conditional Independence Criterion (HSCIC) [Park and Muandet, 2020].

## 2 Preliminaries

**Counterfactual invariance.** We introduce structural causal models as in Pearl [2000].

**Definition 2.1** (Structural causal model (SCM)). A structural causal model is a tuple  $(\mathbf{U}, \mathbf{V}, F, \mathbb{P}_{\mathbf{U}})$  such that

1.  $\mathbf{U}$  is a set of background variables that are exogenous to the model;
2.  $\mathbf{V}$  is a set of observable (endogenous) variables;
3.  $F = \{f_V\}_{V \in \mathbf{V}}$  is a set of functions from (the domains of)  $\text{pa}(V) \cup U_V$  to (the domain of)  $V$ , where  $U_V \subset \mathbf{U}$  and  $\text{pa}(V) \subseteq \mathbf{V} \setminus \{V\}$  such that  $V = f_V(\text{pa}(V), U_V)$ ; (iv)  $\mathbb{P}_{\mathbf{U}}$  is a probability distribution over the domain of  $\mathbf{U}$ . Further, the subsets  $\text{pa}(V) \subseteq \mathbf{V} \setminus \{V\}$  are chosen such that the graph  $\mathcal{G}$  over  $\mathbf{V}$  where the edge  $V' \rightarrow V$  is in  $\mathcal{G}$  if and only if  $V' \in \text{pa}(V)$  is a directed acyclic graph (DAG).

We always denote with  $\mathbf{Y} \subset \mathbf{V}$  the outcome (or prediction target), and with  $\hat{\mathbf{Y}}$  a predictor for that target. The predictor  $\hat{\mathbf{Y}}$  is not strictly part of the SCM, because we get to tune it. However, since it takes inputs from  $\mathbf{V}$ , we often treat it as an observed variable in the SCM. Each SCM implies a unique *observational distribution* over  $\mathbf{V}$  [Pearl, 2000]. However, SCMs allow us to also define interventional distributions. Given a variable  $A \in \mathbf{V}$ , an intervention  $A \leftarrow a$  amounts to replacing  $f_A$  in  $F$  with the constant function  $A = a$ . This yields a new SCM, which induces the *interventional distribution*. Similarly, we can intervene on multiple variables  $\mathbf{V} \supseteq \mathbf{A} \leftarrow \mathbf{a}$ . We then write  $\mathbf{Y}_{\mathbf{a}}^*$  for the outcome in the intervened SCM, also called potential outcome. Note that the interventional distribution  $\mathbb{P}_{\mathbf{Y}_{\mathbf{a}}^*}(\mathbf{y})$  differs in general from the conditional distribution  $\mathbb{P}_{\mathbf{Y}|\mathbf{A}}(\mathbf{y} | \mathbf{a})$ , due to possible unobserved confounding effects. We can also condition on a set of

variables  $\mathbf{W} \subseteq \mathbf{V}$  in the (observational distribution of the) original SCM before performing an intervention, which we denote by  $\mathbb{P}_{\mathbf{Y}_{\mathbf{a}}^*|\mathbf{W}}(\mathbf{y} \mid \mathbf{w})$ . This is a counterfactual distribution: “Given that we have observed  $\mathbf{W} = \mathbf{w}$ , what would  $\mathbf{Y}$  have been had we set  $\mathbf{A} \leftarrow \mathbf{a}$ , instead of the values  $\mathbf{A}$  had actually taken?”. Note that the sets  $\mathbf{A}$  and  $\mathbf{W}$  need not be disjoint. We can now define counterfactual invariance.

**Definition 2.2** (Counterfactual invariance). Let  $\mathbf{A}, \mathbf{W}$  be (not necessarily disjoint) sets of nodes in a given SCM. A predictor  $\hat{\mathbf{Y}}$  is counterfactually invariant in  $\mathbf{A}$  with respect to  $\mathbf{W}$  if  $\mathbb{P}_{\hat{\mathbf{Y}}_{\mathbf{a}}^*|\mathbf{W}}(\mathbf{y} \mid \mathbf{w}) = \mathbb{P}_{\hat{\mathbf{Y}}_{\mathbf{a}'}^*|\mathbf{W}}(\mathbf{y} \mid \mathbf{w})$  almost surely, for all  $\mathbf{a}, \mathbf{a}'$  in the domain of  $\mathbf{A}$ , and all  $\mathbf{w}$  in the domain of  $\mathbf{W}$ .<sup>1</sup>

A predictor that is counterfactually invariant can thus be viewed as robust to changes of  $\mathbf{A}$ , in the sense that the (conditional) post-interventional distribution of  $\hat{\mathbf{Y}}$  does not change for different values of the intervention. In other words, the classification would not change had we gone back and changed the position of the object. This definition is stronger than previous definitions of counterfactual invariance (see Definition 1.1 by Veitch et al. [2021]). In fact, the invariance notion by Veitch et al. [2021] only requires  $\mathbb{P}_{\hat{\mathbf{Y}}_{\mathbf{a}}^*}(\mathbf{y}) = \mathbb{P}_{\hat{\mathbf{Y}}_{\mathbf{a}'}^*}(\mathbf{y})$  almost surely, for all  $\mathbf{a}, \mathbf{a}'$  in the domain of  $\mathbf{A}$ .

**Kernel mean embeddings and conditional measures.** Our regularization term heavily relies on kernel mean embeddings (KMEs). We now highlight the main concepts pertaining KMEs and refer the reader to Berlinet and Thomas-Agnan [2011], Muandet et al. [2017], Schölkopf et al. [2002], Smola et al. [2007] for more details. Fix a measurable space  $\mathcal{Y}$  with respect to a  $\sigma$ -algebra  $\mathcal{F}_{\mathcal{Y}}$ , and consider a probability measure  $\mathbb{P}$  on the space  $(\mathcal{Y}, \mathcal{F}_{\mathcal{Y}})$ . Let  $\mathcal{H}$  be a reproducing kernel Hilbert space (RKHS) with a bounded kernel  $k_{\mathbf{Y}}: \mathcal{Y} \times \mathcal{Y} \rightarrow \mathbb{R}$ , i.e.,  $k_{\mathbf{Y}}$  is such that  $\sup_{\mathbf{y} \in \mathcal{Y}} k(\mathbf{y}, \mathbf{y}) < +\infty$ . The kernel mean embedding  $\mu_{\mathbb{P}}$  of  $\mathbb{P}$  is defined as the expected value of the function  $k(\cdot, \mathbf{y})$  with respect to  $\mathbf{y}$ , i.e.,  $\mu_{\mathbb{P}} := \mathbb{E}[k(\cdot, \mathbf{y})]$ .

The definition of KMEs can be extended to conditional distributions [Fukumizu et al., 2013, Grünewälder et al., 2012, Song et al., 2013, 2009]. Consider two random variables  $\mathbf{Y}, \mathbf{Z}$ , and denote with  $(\Omega_{\mathbf{Y}}, \mathcal{F}_{\mathbf{Y}})$  and  $(\Omega_{\mathbf{Z}}, \mathcal{F}_{\mathbf{Z}})$  the respective measurable spaces. These random variables induce a probability measure  $\mathbb{P}_{\mathbf{Y}, \mathbf{Z}}$  in the product space  $\Omega_{\mathbf{Y}} \times \Omega_{\mathbf{Z}}$ . Let  $\mathcal{H}_{\mathbf{Y}}$  be a RKHS with a bounded kernel  $k_{\mathbf{Y}}(\cdot, \cdot)$  on  $\Omega_{\mathbf{Y}}$ . We define the KME of a conditional distribution  $\mathbb{P}_{\mathbf{Y}|\mathbf{Z}}(\cdot \mid \mathbf{z})$  via  $\mu_{\mathbf{Y}|\mathbf{Z}=\mathbf{z}} := \mathbb{E}[k_{\mathbf{Y}}(\cdot, \mathbf{y}) \mid \mathbf{Z} = \mathbf{z}]$ . Here, the expected value is taken over  $\mathbf{y}$ . KMEs of conditional measures can be estimated from samples. To illustrate this, consider i.i.d. samples  $(\mathbf{y}_1, \mathbf{z}_1), \dots, (\mathbf{y}_n, \mathbf{z}_n)$ . Denote with  $\hat{K}_{\mathbf{Y}}$  the kernel matrix with entries  $[\hat{K}_{\mathbf{Y}}]_{i,j} := k_{\mathbf{Y}}(\mathbf{y}_i, \mathbf{y}_j)$ . Furthermore, let  $k_{\mathbf{Z}}$  be a bounded kernel on  $\Omega_{\mathbf{Z}}$ . Then,  $\mu_{\mathbf{Y}|\mathbf{Z}=\mathbf{z}}$  can be estimated as

$$\hat{\mu}_{\mathbf{Y}|\mathbf{Z}=\mathbf{z}} := \sum_{i=1}^n \hat{w}_{\mathbf{Y}|\mathbf{Z}}^{(i)}(\mathbf{z}) k_{\mathbf{Y}}(\cdot, \mathbf{y}_i) \quad \text{with} \quad \hat{w}_{\mathbf{Y}|\mathbf{Z}}(\cdot) := (\hat{K}_{\mathbf{Z}} - n\lambda I)^{-1} [k_{\mathbf{Z}}(\cdot, \mathbf{z}_1), \dots, k_{\mathbf{Z}}(\cdot, \mathbf{z}_n)]^T \quad (1)$$

where,  $I$  is the identity matrix and  $\lambda$  is a regularization parameter. Here,  $\hat{w}_{\mathbf{X}|\mathbf{A}}^{(i)}(\cdot)$ , the  $i$ -th entry of  $\hat{w}_{\mathbf{X}|\mathbf{A}}(\cdot)$ , are the coefficients of kernel ridge regression [Grünewälder et al., 2012].

### 3 Counterfactually invariant predictors

**Counterfactual invariance from conditional independence.** In this section, we establish a simple graphical criterion to express the desired counterfactual invariance as a conditional independence in the observational distribution, rendering it estimable from i.i.d. data. We first repeat the notion of *blocked paths* [Pearl, 2000].

<sup>1</sup>With a mild abuse of notation, if  $\mathbf{W} = \emptyset$  then the requirement of conditional counterfactual invariance becomes  $\mathbb{P}_{\hat{\mathbf{Y}}_{\mathbf{a}}^*}(\mathbf{y}) = \mathbb{P}_{\hat{\mathbf{Y}}_{\mathbf{a}'}^*}(\mathbf{y})$  almost surely, for all  $\mathbf{a}, \mathbf{a}'$  in the domain of  $\mathbf{A}$ .

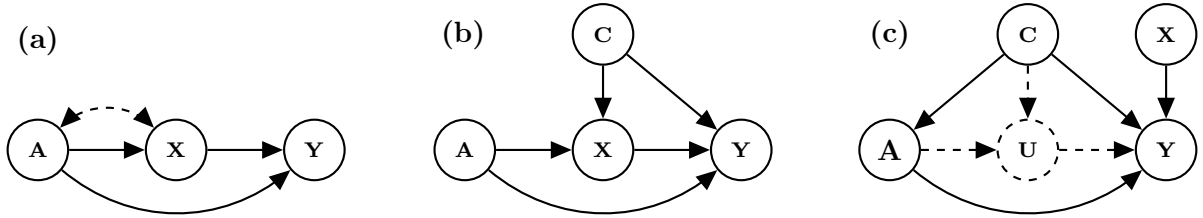


Figure 1: **(a) An example for 3.2**, where  $\mathbb{P}_{\mathbf{Y}_a^*}(\mathbf{y})$  is unidentifiable, due to the confounding effect denoted by the dashed double arrow. However, by 3.2 any predictor  $\hat{\mathbf{Y}}$  such that  $\hat{\mathbf{Y}} \perp\!\!\!\perp \mathbf{A} \mid \mathbf{Z}$  with  $\mathbf{Z} = \{\mathbf{X}\}$  is counterfactually invariant in  $\mathbf{A}$ . Hence, the criterion in 3.2 is weaker than identifiability. **(b) Assumed causal structure for the Adult dataset**, where  $\mathbf{A}$  consists of the protected attributes *gender* and *age*. A predictor is learned for the income  $\mathbf{Y}$  that is invariant in  $\mathbf{A}$ , which corresponds to counterfactual fairness (see 4.1). **(c) Causal structure for the constructed dSprites ground truth**, where  $\mathbf{A} = \{\text{Pos.X}\}$ ,  $\mathbf{U} = \{\text{Scale}\}$ ,  $\mathbf{C} = \{\text{Shape, Pos.Y}\}$ ,  $\mathbf{X} = \{\text{Color, Orientation}\}$ , and  $\mathbf{Y} = \{\text{Outcome}\}$ .  $\mathbf{U}$  is unobserved. We want a predictor for  $\mathbf{Y}$ , which is counterfactually invariant in  $\mathbf{A}$  with respect to all other observed attributes (see 4).

**Definition 3.1.** Consider a path  $\pi$  of causal graph  $\mathcal{G}$ . A set of nodes  $\mathbf{Z}$  blocks  $\pi$ , if  $\pi$  contains a triple of consecutive nodes connected in one of the following ways:  $N_i \rightarrow Z \rightarrow N_j$ ,  $N_i \leftarrow Z \rightarrow N_j$ , or  $N_i \rightarrow M \leftarrow N_j$ , with  $N_i, N_j \notin \mathbf{Z}$ ,  $Z \in \mathbf{Z}$ , and neither  $M$  nor any descendent of  $M$  is in  $\mathbf{Z}$ .

Using 3.1, we give the following criterion for counterfactual invariance.

**Theorem 3.2.** Let  $\mathcal{G}$  be a causal diagram, and consider two (not necessarily disjoint) sets of nodes  $\mathbf{A}$ ,  $\mathbf{W}$ . Let  $\mathbf{Z}$  be a set of nodes that blocks all non-directed paths from  $\mathbf{A} \cup \mathbf{W}$  to  $\mathbf{Y}$ . Then, for any SCM compatible with  $\mathcal{G}$ , any predictor  $\hat{\mathbf{Y}}$  that satisfies  $\hat{\mathbf{Y}} \perp\!\!\!\perp \mathbf{A} \mid \mathbf{Z}$  is counterfactually invariant in  $\mathbf{A}$  with respect to  $\mathbf{W}$ .

The proof is deferred to Appendix A, where we derive the graphical criterion by studying a graphical model similar to the counterfactual graph [Shpitser and Pearl, 2008]. Our key observation is that the set  $\mathbf{Z}$  as in 3.2 acts as a valid adjustment set for certain random variables in this joint pre- and post-interventional graphical model. Using this observation, we derive A.3 with similar techniques to covariate adjustment. However, our proof does *not* achieve identification of the counterfactual distributions by simply applying the do-calculus [Pearl, 2000]. Crucially, *the existence of a measurable set  $\mathbf{Z}$  as in Theorem 3.2 does not imply the identifiability of counterfactual distributions  $\mathbb{P}_{\mathbf{Y}_a^*}(\mathbf{y})$*  (see Figure 1(a) for a counterexample). In particular, Theorem 3.2 does not rule out hidden confounding in the model. Hence, our method is applicable when (certain parameters of)  $\mathbb{P}_{\mathbf{Y}_a^*}(\mathbf{y})$  or  $\mathbb{P}_{\mathbf{Y}_a^*|\mathbf{W}}(\mathbf{y})$  cannot be learned from observational data.

**Counterfactually invariant predictors.** We now propose our novel regularization term denoted by  $\text{HSCIC}(\hat{\mathbf{Y}}, \mathbf{A} \mid \mathbf{Z})$  that promotes counterfactual invariance by encouraging the conditional independence  $\hat{\mathbf{Y}} \perp\!\!\!\perp \mathbf{A} \mid \mathbf{Z}$  (see Theorem 3.2). Given a loss function  $\mathcal{L}(\hat{\mathbf{Y}})$  for the predictive performance of  $\hat{\mathbf{Y}}$ , we propose to minimize the following loss

$$\mathcal{L}_{\text{TOTAL}}(\hat{\mathbf{Y}}) = \mathcal{L}(\hat{\mathbf{Y}}) + \gamma \cdot \text{HSCIC}(\hat{\mathbf{Y}}, \mathbf{A} \mid \mathbf{Z}), \quad (2)$$

with a regularization parameter  $\gamma \geq 0$ . We will now develop and justify the regularization term (see Corollary 3.5) for which  $\text{HSCIC}(\hat{\mathbf{Y}}, \mathbf{A} \mid \mathbf{Z}) = 0$  if and only if  $\hat{\mathbf{Y}} \perp\!\!\!\perp \mathbf{A} \mid \mathbf{Z}$ .

**Hilbert-Schmidt Conditional Independence Criterion (HSCIC).** Consider two random variables  $\mathbf{Y}$  and  $\mathbf{A}$ , and denote with  $(\Omega_{\mathbf{Y}}, \mathcal{F}_{\mathbf{Y}})$  and  $(\Omega_{\mathbf{A}}, \mathcal{F}_{\mathbf{A}})$  the respective measurable spaces. Suppose that we are given two RKHSs  $\mathcal{H}_{\mathbf{Y}}$ ,  $\mathcal{H}_{\mathbf{A}}$  over the support of  $\mathbf{Y}$  and  $\mathbf{A}$  respectively. The tensor product space  $\mathcal{H}_{\mathbf{Y}} \otimes \mathcal{H}_{\mathbf{A}}$  is defined as the space of functions of the form

$(f \otimes g)(\mathbf{y}, \mathbf{a}) := f(\mathbf{y})g(\mathbf{a})$ , for all  $f \in \mathcal{H}_{\mathbf{Y}}$  and  $g \in \mathcal{H}_{\mathbf{A}}$ . The tensor product space yields a natural RKHS structure, with kernel  $k$  defined by  $k(\mathbf{y} \otimes \mathbf{a}, \mathbf{y}' \otimes \mathbf{a}') := k_{\mathbf{Y}}(\mathbf{y}, \mathbf{y}')k_{\mathbf{A}}(\mathbf{a}, \mathbf{a}')$ . We refer the reader, i.e., to [Szabó and Sriperumbudur \[2017\]](#) for more details on tensor product spaces. With this notation we define:

**Definition 3.3** (HSCIC). For (sets of) random variables  $\mathbf{Y}, \mathbf{A}, \mathbf{Z}$  the HSCIC between  $\mathbf{Y}$  and  $\mathbf{A}$  given  $\mathbf{Z}$  is defined as the real-valued random variable  $\text{HSCIC}(\mathbf{Y}, \mathbf{A} \mid \mathbf{Z}) = H_{\mathbf{Y}, \mathbf{A} \mid \mathbf{Z}} \circ \mathbf{Z}$ . Here,  $H_{\mathbf{Y}, \mathbf{A} \mid \mathbf{Z}}$  is a real-valued deterministic function, defined as

$$H_{\mathbf{Y}, \mathbf{A} \mid \mathbf{Z}}(\mathbf{z}) := \left\| \mu_{\mathbf{Y}, \mathbf{A} \mid \mathbf{Z}=\mathbf{z}} - \mu_{\mathbf{Y} \mid \mathbf{Z}=\mathbf{z}} \otimes \mu_{\mathbf{A} \mid \mathbf{Z}=\mathbf{z}} \right\|,$$

with  $\|\cdot\|$  the metric induced by the inner product of the tensor product space  $\mathcal{H}_{\mathbf{X}} \otimes \mathcal{H}_{\mathbf{A}}$ .

The HSCIC has the following important property.

**Theorem 3.4.** *With the notation introduced above, suppose that the kernel  $k$  of the tensor product space  $\mathcal{H}_{\mathbf{X}} \otimes \mathcal{H}_{\mathbf{A}}$  is characteristic.<sup>2</sup> Then,  $\text{HSCIC}(\mathbf{Y}, \mathbf{A} \mid \mathbf{Z}) = 0$  almost surely if and only if  $\mathbf{Y} \perp\!\!\!\perp \mathbf{A} \mid \mathbf{Z}$ .*

We provide a proof in [Appendix B](#). The HSCIC as a criterion for conditional independence is not a novel concept [[Park and Muandet, 2020](#)]. However, our definition differs from [Park and Muandet \[2020\]](#), who define the HSCIC via KMEs based on the Bochner conditional expected value. In contrast, we define the HSCIC using the embeddings of conditional measures  $\mu_{\mathbf{Y} \mid \mathbf{Z}=\mathbf{z}}$ . This allows us to bypass some technical assumptions required by [Park and Muandet \[2020\]](#), while retaining generality over cross-covariance based methods [[Fukumizu et al., 2007](#)]. We refer readers to [Appendix C](#) and [D](#) for a comparison with previous approaches. Combining [Theorem 3.2](#) with [Theorem 3.4](#), we can now use the HSCIC to promote counterfactual invariance.

**Corollary 3.5.** *Consider an SCM with causal diagram  $\mathcal{G}$  and fix two (not necessarily disjoint) sets of nodes  $\mathbf{A}, \mathbf{W}$ . Let  $\mathbf{Z}$  be a set of nodes in  $\mathcal{G}$  that blocks all non-directed paths from  $\mathbf{A} \cup \mathbf{W}$  to  $\mathbf{Y}$ . Then, any predictor  $\hat{\mathbf{Y}}$  that satisfies  $\text{HSCIC}(\hat{\mathbf{Y}}, \mathbf{A} \mid \mathbf{Z}) = 0$  almost surely is counterfactually invariant in  $\mathbf{A}$  with respect to  $\mathbf{W}$ .*

**Estimating the HSCIC from samples.** We show how to estimate  $\text{HSCIC}(\mathbf{Y}, \mathbf{A} \mid \mathbf{Z})$  from finite samples using [eq. \(1\)](#). Given  $n$  samples  $\{(\mathbf{y}_i, \mathbf{a}_i, \mathbf{z}_i)\}_{i=1}^n$ , denote by  $\hat{K}_{\mathbf{Y}}$  and  $\hat{K}_{\mathbf{A}}$  the corresponding kernel matrices for  $\mathbf{Y}$  and  $\mathbf{A}$ . We then estimate the  $H_{\mathbf{Y}, \mathbf{A} \mid \mathbf{Z}}$  as [[Park and Muandet, 2020](#)]

$$\begin{aligned} \hat{H}_{\mathbf{Y}, \mathbf{A} \mid \mathbf{Z}}^2(\cdot) &= \hat{w}_{\mathbf{Y}, \mathbf{A} \mid \mathbf{Z}}^T(\cdot) \left( \hat{K}_{\mathbf{Y}} \odot \hat{K}_{\mathbf{A}} \right) \hat{w}_{\mathbf{Y}, \mathbf{A} \mid \mathbf{Z}}(\cdot) - 2 \left( \hat{w}_{\mathbf{Y} \mid \mathbf{Z}}^T(\cdot) \hat{K}_{\mathbf{Y}} \hat{w}_{\mathbf{Y}, \mathbf{A} \mid \mathbf{Z}}(\cdot) \right) \\ &\quad \cdot \left( \hat{w}_{\mathbf{A} \mid \mathbf{Z}}^T(\cdot) \hat{K}_{\mathbf{A}} \hat{w}_{\mathbf{Y}, \mathbf{A} \mid \mathbf{Z}}(\cdot) \right) + \left( \hat{w}_{\mathbf{Y} \mid \mathbf{Z}}^T(\cdot) \hat{K}_{\mathbf{Y}} \hat{w}_{\mathbf{Y} \mid \mathbf{Z}}(\cdot) \right) \left( \hat{w}_{\mathbf{A} \mid \mathbf{Z}}^T(\cdot) \hat{K}_{\mathbf{A}} \hat{w}_{\mathbf{A} \mid \mathbf{Z}}(\cdot) \right), \end{aligned} \quad (3)$$

where  $\odot$  is element-wise multiplication. As mentioned, the vectors  $\hat{w}_{\mathbf{Y} \mid \mathbf{Z}}(\cdot)$ ,  $\hat{w}_{\mathbf{A} \mid \mathbf{Z}}(\cdot)$ , and  $\hat{w}_{\mathbf{Y}, \mathbf{A} \mid \mathbf{Z}}(\cdot)$  are found via kernel ridge regression. [Theorem 1](#) by [Caponnetto and Vito \[2007\]](#) shows that if the regularization parameters for the kernel ridge coefficients decay to 0 sufficiently quickly as  $n \rightarrow \infty$ , then  $\hat{H}_{\mathbf{Y}, \mathbf{A} \mid \mathbf{Z}}^2(\cdot)$  converges to  $H_{\mathbf{Y}, \mathbf{A} \mid \mathbf{Z}}^2(\cdot)$  at a rate of  $n^{-c}$ , where  $c$  is a parameter depending on the complexity of the embeddings and the effective dimensions of  $\mathcal{H}_{\mathbf{Y}}$  and  $\mathcal{H}_{\mathbf{A}}$ . In practice, computing the HSCIC approximation  $\hat{H}_{\mathbf{Y}, \mathbf{A} \mid \mathbf{Z}}^2(\cdot)$  may be time-consuming. To speed it up, we can use random Fourier features to approximate the matrices  $\hat{K}_{\mathbf{Y}}$  and  $\hat{K}_{\mathbf{A}}$  as above [[Avron et al., 2017](#), [Rahimi and Recht, 2007](#)]. We refer readers to [Appendix E](#) for a discussion of the use of random Fourier features.

<sup>2</sup>The tensor product kernel  $k$  is characteristic if the mapping  $\mathbb{P}_{\mathbf{Y}, \mathbf{A}} \mapsto \mathbb{E}[k(\cdot, \mathbf{y} \otimes \mathbf{a})]$  is injective. Here, the expected value is taken over the pair  $(\mathbf{y}, \mathbf{a})$ .



**Measuring counterfactual invariance.** Besides predictive performance, e.g., mean squared error (**MSE**) for regression, our key metric of interest is the level of counterfactual invariance achieved by the predictor  $\hat{\mathbf{Y}}$ . We quantify the overall counterfactual variance as a single scalar

$$\mathbf{VCF}(\hat{\mathbf{Y}}) = \mathbb{E}_{\mathbf{w} \sim \mathbb{P}_{\mathbf{W}}} \left[ \text{var}_{\mathbf{a}' \sim \mathbb{P}_{\mathbf{A}}} \left[ \mathbb{E}_{\hat{\mathbf{Y}}_{\mathbf{a}'}} | \mathbf{w} (\hat{\mathbf{y}} | \mathbf{w}) \right] \right]. \quad (4)$$

For deterministic predictors (i.e., point estimators), which we use in all our experiments, the variance term is zero if and only if counterfactual invariance holds at  $\mathbf{w}$  for (almost) all  $\mathbf{a}'$  in the support of  $\mathbb{P}_{\mathbf{A}}$  (i.e., the prediction remains constant). Since the variance is non-negative, **VCF** (we often drop the argument) is zero if and only if counterfactual invariance holds almost surely. However, the outer expectation of **VCF** may still be sensitive to outliers in its arguments, which is why it can be instructive to also analyze the variances for different conditioning values  $\mathbf{Z} = \mathbf{z}$ . To estimate **VCF** in practice, we pick  $d$  datapoints  $(\mathbf{w}_i)_{i=1}^d$  from the observed data, and for each compute the counterfactual outcomes  $\hat{\mathbf{Y}}_{\mathbf{a}'}^* | \mathbf{w}_i$  for  $k$  different values of  $\mathbf{a}'$ . The inner expectation is simply the predictor output. We use empirical variances with  $k$  examples for each of the  $d$  chosen datapoints, and the empirical mean of the  $d$  variances for the outer expectation. Finally, we note that by 3.5, HSCIC itself also serves as a useful measure of how well counterfactual invariance has been enforced.

## 4 Applications of counterfactual invariance

To clarify the benefits and challenges of counterfactual invariance, we now provide brief explanations of potential application areas, which we will subsequently study empirically with real-world data.

**Image classification.** Counterfactual invariance serves as a strong notion of robustness in high-dimensional settings, such as image classification: “Would the truck have been classified correctly had it been winter in this exact situation instead of summer?” For concrete demonstration, we use the dSprites dataset [Matthey et al., 2017], which consists of relatively simple, yet high-dimensional, square black and white images of different shapes (squares, ellipses, etc.), sizes, and orientations (rotation) in different xy-positions (see Figure 2). Since this dataset is fully synthetic and labelled (we know all factors for each image), we consider a causal model as depicted in Figure 1(c). The full structural equations are provided in Appendix F.4. The main goal in this application is to evaluate our method for high-dimensional data, including mixed categorical (e.g., shapes) and continuous (e.g., position) variables. Therefore, we set the outcome  $\mathbf{Y}$  to be a function of all observed and unobserved variables, which can be inferred from the high-dimensional images.

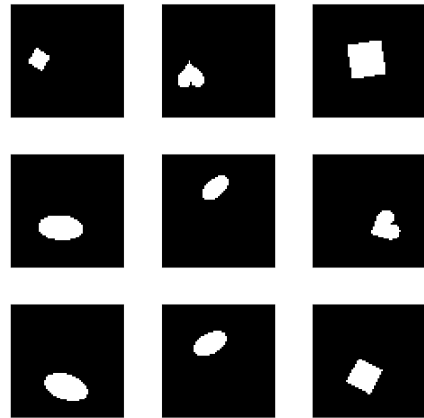


Figure 2: **Examples of images from the dSprites dataset** [Matthey et al., 2017]. This dataset consists of 2D shapes generated from 6 ground truth independent latent factors.

**Counterfactual fairness.** We first show that the popular definition of counterfactual fairness [Kusner et al., 2017] is an incarnation of counterfactual invariance (see Definition 2.2). Counterfactual fairness corresponds to the commonly posed question, after receiving a consequential decision from an algorithm: “Would I have gotten the same outcome had I been a different gender, race, or age with all else being equal?”. Again, we denote the outcome by  $\mathbf{Y} \subset \mathbf{V}$  and so-called *protected attributes* by  $\mathbf{A} \subseteq \mathbf{V} \setminus \mathbf{Y}$ . These attributes typically constitute demographic features such as gender, race, or age protected under anti-discrimination laws (see, e.g., Barocas

and Selbst [2016]). Collecting all remaining observed covariates into  $\mathbf{W} := \mathbf{V} \setminus \mathbf{Y}$ , we define counterfactual fairness as follows, showing that it is a special case of counterfactual invariance.

**Definition 4.1** (Counterfactual Fairness, Definition 5 by Kusner et al. [2017]). A predictor  $\hat{\mathbf{Y}}$  is counterfactually fair if under any context  $\mathbf{W} = \mathbf{w}$  and  $\mathbf{A} = \mathbf{a}$ , it holds  $\mathbb{P}_{\hat{\mathbf{Y}}_{\mathbf{a}}^* | \mathbf{W}, \mathbf{A}}(\mathbf{y} | \mathbf{w}, \mathbf{a}) = \mathbb{P}_{\hat{\mathbf{Y}}_{\mathbf{a}'} | \mathbf{W}, \mathbf{A}}(\mathbf{y} | \mathbf{w}, \mathbf{a})$ , for all  $\mathbf{y}$  and for any value  $\mathbf{a}'$  attainable by  $\mathbf{A}$ .

For a concrete example, we consider the commonly used ‘‘Adult’’ dataset from the UCI repository [Kohavi and Becker, 1996]. Our goal is to predict whether an individual’s income is above a certain threshold  $\mathbf{Y} \in \{0, 1\}$  based on a collection of (demographic) information including protected attributes such as gender and age. From a fairness perspective, such a predictor could be used in loan-granting decisions, where one must not discriminate against certain demographic groups. We follow Chiappa [2019], Nabi and Shpitser [2018], where a subset of variables are selected from the dataset and a causal structure is assumed as in Figure 1(b). We choose gender (considered binary in this dataset) and age (considered continuous) as the protected attributes  $\mathbf{A}$ . We denote the marital status, level of education, occupation, working hours per week, and work class jointly by  $\mathbf{X}$  and combine the remaining observed attributes in  $\mathbf{C}$ . With this notation, our goal is to learn a predictor  $\hat{\mathbf{Y}}$  that is counterfactually invariant (or fair) in  $\mathbf{A}$  with respect to  $\mathbf{W} = \mathbf{C} \cup \mathbf{X}$ . We remark that achieving fairness for continuous or even mixed categorical and continuous protected attributes is an ongoing line of research (even for non-causal fairness notions) [Chiappa and Pacchiano, 2021, Mary et al., 2019], but directly supported by HSCIC.

## 5 Experiments

We begin our empirical assessment of HSCIC on synthetic datasets, where ground truth is known and systematically study how performance is influenced by the dimensionality of the variables. We then move to the dSprites and Adult datasets described in 4.

### 5.1 Synthetic experiments

We simulate different datasets following to the causal graphical structure in Figure 3. The datasets are composed of four sets of observed continuous variables (i) the prediction target  $\mathbf{Y}$ , (ii) the variable(s) we want to be counterfactually invariant in  $\mathbf{A}$ , (iii) observed covariates that mediate effects from  $\mathbf{A}$  on  $\mathbf{Y}$ , and (iv) observed confounding variables  $\mathbf{Z}$ . The goal is to learn a predictor  $\hat{\mathbf{Y}}$  that is counterfactually invariant in  $\mathbf{A}$  with respect to  $\mathbf{W} := \mathbf{A} \cup \mathbf{X} \cup \mathbf{Z}$ . We consider various artificially generated datasets for this example, which mainly differ in the dimension of the observed variables and their correlations. A detailed description of each dataset is deferred to Appendix F.

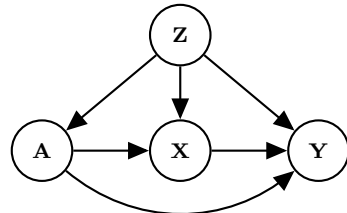


Figure 3: **Assumed causal structure for the synthetic experiments** (see Section 5.1). The precise corresponding generative random variables are described in Appendix F.

For all synthetic experiments, we train the model using fully connected networks (MLPs). We use the MSE loss  $\mathcal{L}_{\text{MSE}}(\hat{\mathbf{Y}})$  as the predictive loss  $\mathcal{L}$  in eq. (2) for continuous outcomes  $\mathbf{Y}$ . We generate 4k samples from the observational distribution in each setting and use a 80:20 train/test split. All metrics reported are on the test set. We perform hyper-parameter tuning for MLP hyperparameters based on a random strategy (see Appendix F for details). The  $\text{HSCIC}(\hat{\mathbf{Y}}, \mathbf{A} | \mathbf{Z})$  term is computed as in eq. (3) using a Gaussian kernel with amplitude 1.0 and length scale 0.1. The regularization parameter  $\lambda$  for the ridge regression coefficients in eq. (1) is set to  $\lambda = 0.01$ . To estimate  $\mathbf{VCF}$  we set  $d = 1000$  and  $k = 500$ .

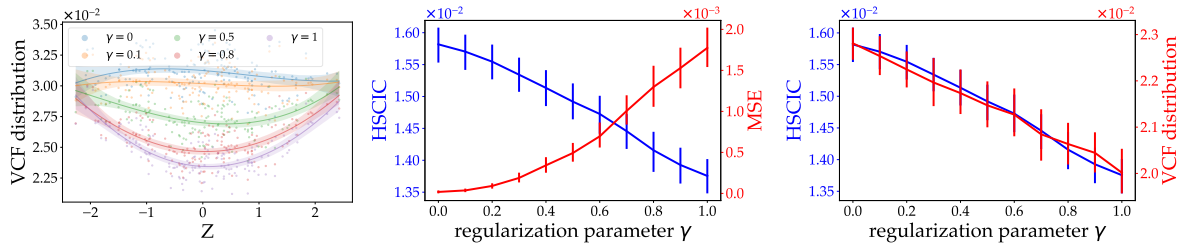


Figure 4: **(Left) variance of the counterfactual distributions** for  $d = 100$  datapoints with lines representing 3<sup>rd</sup>-order polynomial regression and shaded areas being 95% confidence intervals. **(Center) trade-off between accuracy and counterfactual invariance.** We observe that the HSCIC decreases, as the MSE increases. Vertical bars denote standard errors over 15 different random seeds. **(Right) Correspondence between the HSCIC and the VCF**, for increasing regularizer  $\gamma$ . Again, vertical bars denote standard errors over 15 different random seeds.

**Model performance with the use of the HSCIC.** We first perform a set of experiments to study the effect of the HSCIC, and to highlight the trade-off between accuracy and counterfactual invariance. For this set of experiments, we generate a dataset as described in Appendix F.1. Figure 4 (left) shows the **VCF** for different regularization parameters  $\gamma$ , as a function of the values of  $\mathbf{Z}$ . We observe that increasing values of  $\gamma$  lead to a consistent decrease of **VCF**. Figure 4 (center) shows the values attained by the HSCIC and **MSE** for increasing parameter  $\gamma$ , demonstrating the expected trade-off in raw predictive performance and enforcing counterfactual invariance. Finally, Figure 4 (right) highlights the usefulness of HSCIC as a measure of counterfactual invariance, being in strong agreement with **VCF**.

**Comparison with baselines.** We perform a second set of experiments to compare our method against baselines. For this set of experiments we consider two settings, which we refer to as Scenario 1 and Scenario 2. These two settings differ in how the conditioning set  $\mathbf{Z}$  affects the outcome  $\mathbf{Y}$ , with Scenario 1 exhibiting higher correlation of  $\mathbf{Z}$  with both the mediator  $\mathbf{X}$  and the outcome  $\mathbf{Y}$ . We refer the reader to Appendix F.2 for a precise description of Scenario 1 and Scenario 2. We remark that counterfactually invariant training has not received much attention yet. This limits the choice of baselines for experimental comparison. The main work on this topic to date does not provide a suitable benchmark for experimental comparison [Veitch et al., 2021]. In fact, the method by Veitch et al. [2021] applies to a weaker notion of counterfactual invariance, and it can be used only on specific graphical structures which differ from our set-up. However, since counterfactual fairness is a special case of counterfactual invariance, we can compare to two methods proposed by Kusner et al. [2017] (in applicable settings). We compare to the *Level 1* (only use non-descendants of  $\mathbf{A}$  as inputs to  $\hat{\mathbf{Y}}$ ) and the *Level 3* (assume an additive noise model and in addition to non-descendants, only use the residuals of descendants of  $\mathbf{A}$  after regression on  $\mathbf{A}$  as inputs to  $\hat{\mathbf{Y}}$ ) approaches of Kusner et al. [2017]. We refer to these two baselines as CF1 and CF2 respectively. Note that CF1 satisfies counterfactual invariance perfectly by construction. We compare our method against CF1 and CF2 on both Scenario 1 and Scenario 2. We summarize the results in Table 1. For a suitable choice of  $\gamma$ , our method outperforms the baseline CF2 in both **MSE** and **VCF** simultaneously.

**Multi-dimensional variables.** We perform a third set of experiments to assess HSCIC’s performance in higher dimensions. We consider simulated datasets as described in Appendix F.3. In this set of experiments, we independently increase the dimension of  $\mathbf{Z}$  and  $\mathbf{A}$  in two different simulations, leaving the rest of the variables unchanged. Tables 2 and 3 present the results for different regularization coefficients  $\gamma$  and different dimensions of  $\mathbf{A}$  and  $\mathbf{Z}$ . These results demonstrate that HSCIC can handle multi-dimensional variables while maintaining performance, as counterfactual invariance is approached when  $\gamma$  increases.



Table 1: **Performance of the HSCIC against baselines** CF1 and CF2 on two synthetic datasets (see Appendix F.2). Notably, for  $\gamma = 5$  in Scenario 1 and  $\gamma = 13$  in Scenario 2 we outperform CF2 in **MSE** and **VCF** simultaneously.

	Scenario 1		Scenario 2	
	<b>MSE</b> $\times 10^3$	<b>VCF</b> $\times 10^3$	<b>MSE</b> $\times 10^3$	<b>VCF</b> $\times 10^3$
$\gamma = 0$	$0.36 \pm 0.5$	$20.33 \pm 1$	$2 \pm 0.1$	$239 \pm 0.4$
$\gamma = 5$	$16.97 \pm 2$	$6.84 \pm 1$	$43 \pm 8$	$230 \pm 6$
$\gamma = 10$	$19.80 \pm 2$	$5.89 \pm 0.6$	$50 \pm 8$	$190 \pm 3$
$\gamma = 13$	$22 \pm 1$	$5.78 \pm 0.5$	$133 \pm 6$	$157 \pm 7$
CF1	$24.44 \pm 3$	0	$218 \pm 10$	0
CF2	$19.50 \pm 2$	$7.50 \pm 1$	$137 \pm 4$	$167 \pm 2$

Table 2: **Results of the MSE ( $\times 10^5$  for readability), HSCIC, VCF for increasing dimension of  $\mathbf{A}$** , on a synthetic dataset as in Appendix F.3. In this case, the dimension of the other variables are  $\dim Z = 1, \dim X = 1, \dim Y = 1$ .

$\gamma$	dimA=2			dimA=5			dimA=10			dimA=20		
	<b>MSE</b>	<b>HSCIC</b>	<b>VCF</b>	<b>MSE</b>	<b>HSCIC</b>	<b>VCF</b>	<b>MSE</b>	<b>HSCIC</b>	<b>VCF</b>	<b>MSE</b>	<b>HSCIC</b>	<b>VCF</b>
0	35	0.0230	0.025	1.53	0.0177	0.013	10	0.0150	0.004	1.45	0.0126	0.0010
$\frac{1}{2}$	86	0.0214	0.022	1580	0.0157	0.010	40	0.0135	0.002	33	0.0115	0.0004
1	210	0.0200	0.220	1450	0.0144	0.008	100	0.0127	0.001	60	0.0111	0.0003

## 5.2 High-dimensional image experiments

We perform a set of experiments on a high-dimensional real-world dataset. We consider the image classification task as described in 4. In this set of experiments, we use the dSprites dataset with a causal graph as in Figure 1(c). The full structural equations are provided in Appendix F.4, where we assume a causal graph over the determining factors of the image, and essentially look up the corresponding image in the simulated dataset. This experiment is particularly challenging due to the mixed categorical and continuous variables in  $\mathbf{C}$  (**shape**, **y-pos**) and  $\mathbf{X}$  (**color**, **orientation**), continuous  $\mathbf{A}$  (**x-pos**). All variables except for scale are assumed to be observed, and all variables jointly with the actual image determine the outcome  $\mathbf{Y}$ . Our goal is to learn a predictor  $\hat{\mathbf{Y}}$  that is counterfactually invariant in the x-position with respect to all other observed variables. In the chosen causal structure,  $\{\mathbf{shape}, \mathbf{y-pos}\} \in \mathbf{C}$  block all non-directed paths from  $\mathbf{A} \cup \mathbf{C} \cup \mathbf{U}$  to  $\mathbf{Y}$ . Hence, we seek to achieve  $\hat{\mathbf{Y}} \perp\!\!\!\perp \mathbf{x-pos} \mid \{\mathbf{shape}, \mathbf{y-pos}\}$  via the

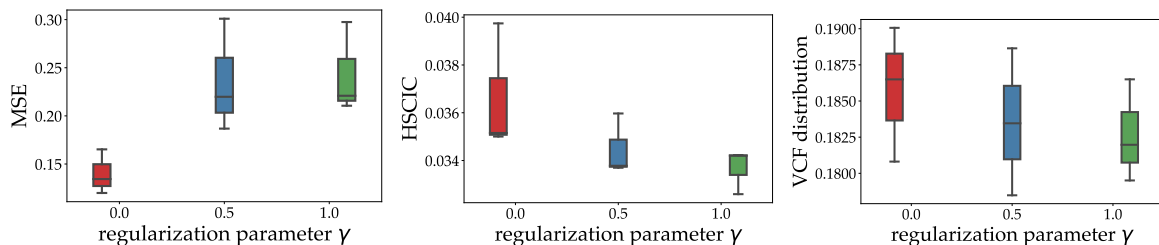
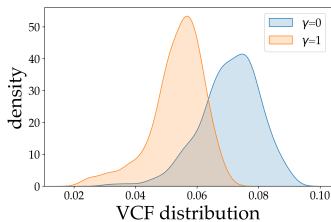


Figure 5: **Results of MSE, HSCIC operator and VCF for the dSprites image dataset experiment.** The HSCIC operator decreases steadily with higher values of  $\gamma$ . Similarly, a necessary increase of **MSE** can be observed. For both  $\gamma = 0.5$  and  $\gamma = 1$  an overall decrease of **VCF** is observed compared to the not-regularized setting. However, probably due to the high dimensional setting, the analysed metrics do not relevantly vary for the two regularized settings.

Table 3: **Results of MSE ( $\times 10^5$  for readability), HSCIC, VCF for increasing dimension of  $\mathbf{Z}$** , on a synthetic dataset as in Appendix F.3. The dimension of the other variables are  $\dim A = 1, \dim X = 1, \dim Y = 1$ .

$\gamma$	dimZ=2			dimZ=3			dimZ=5		
	MSE	HSCIC	VCF	MSE	HSCIC	VCF	MSE	HSCIC	VCF
0	20	0.002024	$6.15 \times 10^{-5}$	11	0.03407	0.023	53.9	0.033180	0.0062
$\frac{1}{2}$	20	0.002023	$1.29 \times 10^{-5}$	49	0.03406	0.016	21.9	0.033178	0.0061
1	20	0.002019	$4.40 \times 10^{-6}$	57	0.03403	0.009	18	0.033176	0.0039



	MSE	HSCIC	VCF
$\gamma = 0$	$(81.725 \pm 0.0481)\%$	$0.01067 \pm 3.4 \times 10^{-5}$	$0.06685 \pm 0.006$
$\gamma = 1$	$(81.547 \pm 0.0745)\%$	$0.00739 \pm 6.8 \times 10^{-5}$	$0.05156 \pm 0.003$

Figure 6: **(Left) Probability density mass of the VCF distribution**, for different choices of  $\gamma$ . We observe less variance and more mass near zero for regularization parameter  $\gamma = 1$ . **(Right) Results of accuracy, HSCIC and VCF**, showing a considerable improvement of HSCIC and VCF for  $\gamma = 1$ .

HSCIC operator. To accommodate the mixed input types,  $\hat{\mathbf{Y}}$  puts an MLP on top of features extracted from the images via convolutional layers concatenated with features extracted from the remaining inputs via an MLP.

Figure 5 demonstrates that HSCIC achieves improved VCF as  $\gamma$  increases up to a certain point while affecting MSE, a necessary trade-off. Adjusting our method to achieve higher stability is an interesting direction for future work.

### 5.3 Fairness with continuous protected attributes

In this experiment we apply our method to the popular UCI Adult dataset [Kohavi and Becker, 1996], described in Section 4. Following previous related work [Chiappa and Pacchiano, 2021], we assume the causal structure depicted in the Appendix F.5. Furthermore, we assume additional latent variables as in Figure 8. Our goal is to learn a classifier for whether

the income of an individual is above a certain threshold, which is counterfactually invariant in both age and gender with respect to a collection of additional demographic attributes. Here, we use an MLP with binary cross-entropy loss for  $\hat{\mathbf{Y}}$ . Since this experiment is based on real data, the true counterfactual distribution cannot be known. For an evaluation of our method, we thus again follow Chiappa and Pacchiano [2021] and estimate a possible true underlying structure by inferring the posterior distribution over the unobserved variables using variational autoencoders [Kingma and Welling, 2014]. Even though this can only provide approximate variances of counterfactual distributions, Figure 6 (left) shows that HSCIC still achieves more counterfactually fair outcome distributions (more mass near zero) than an unconstrained classifier ( $\gamma = 0$ ). Figure 6 (right) highlights once more that the HSCIC operator reliably decreases also in classification setting, again trading off accuracy.

## 6 Discussion and future work

We study the problem of learning predictors  $\hat{Y}$  that are “counterfactually invariant” in changes of certain covariates. We put forth a formal definition of counterfactual invariance and describe how it generalizes existing notions. Next, we provided a novel graphical criterion to characterize counterfactual invariance and reduce it to a conditional independence statement. Our method does not require identifiability of the counterfactual distribution or exclude the possibility of unobserved confounders. Finally, we propose an efficiently estimable, model-agnostic regularization term to enforce this conditional independence based on kernel mean embeddings of conditional measures, which works for mixed continuous/categorical, multi-dimensional variables. We demonstrate the efficacy of our method in regression and classification tasks involving controlled synthetic scenarios, high-dimensional images, and in a fairness application, where it outperforms existing baselines.

The main limitation of our work, as for all studies in this domain, is the assumption that the causal graph is known. Another limitation is that our methodology is applicable when a graphical criterion is satisfied, i.e., the required variables are observed. From an ethics perspective, the increased robustness of counterfactually invariant (or societal benefits of counterfactually fair) predictors are certainly desirable. However, this presupposes that all the often untestable assumptions are valid. Overall, causal methodology should not be applied lightly, especially in high-stakes and consequential decisions. A critical analysis of the broader context or systemic factors may hold more promise for societal benefits, than a well-crafted algorithmic predictor.

In light of the limitations mentioned above, an interesting and important direction for future work is to assess the sensitivity of our method to misspecifications of the causal graph or insufficient knowledge of the required blocking set. Finally, we believe our graphical criterion and KMEs-based regularization can also be useful for causal representation learning, where one aims to isolate causally relevant, autonomous factors underlying the data generating process of high-dimensional data.

### Acknowledgement

This work was supported by the German Federal Ministry of Education and Research (BMBF): Tübingen AI Center, FKZ: 01IS18039B.

## References

- Arjovsky, M., Bottou, L., Gulrajani, I., and Lopez-Paz, D. (2019). Invariant risk minimization. *arXiv preprint arXiv:1907.02893*.
- Avron, H., Kapralov, M., Musco, C., Musco, C., Velingker, A., and Zandieh, A. (2017). Random fourier features for kernel ridge regression: Approximation bounds and statistical guarantees. In *International conference on machine learning*, volume 70, pages 253–262.
- Barocas, S. and Selbst, A. D. (2016). Big data’s disparate impact. *California Law Review*, 104.
- Battaglia, P. W., Hamrick, J. B., Bapst, V., Sanchez-Gonzalez, A., Zambaldi, V., Malinowski, M., Tacchetti, A., Raposo, D., Santoro, A., Faulkner, R., et al. (2018). Relational inductive biases, deep learning, and graph networks. *arXiv preprint arXiv:1806.01261*.
- Berlinet, A. and Thomas-Agnan, C. (2011). *Reproducing kernel Hilbert spaces in probability and statistics*. Springer Science & Business Media.
- Bloem-Reddy, B. and Teh, Y. W. (2020). Probabilistic symmetries and invariant neural networks. *The Journal of Machine Learning Research*, 21:90–1.

- Bühlmann, P. (2020). Invariance, causality and robustness. *Statistical Science*, 35(3):404–426.
- Caponnetto, A. and Vito, E. D. (2007). Optimal rates for the regularized least-squares algorithm. *Foundations of Computational Mathematics*, 7(3):331–368.
- Chen, T., Kornblith, S., Norouzi, M., and Hinton, G. (2020). A simple framework for contrastive learning of visual representations. In *International conference on machine learning*, pages 1597–1607. PMLR.
- Chiappa, S. (2019). Path-specific counterfactual fairness. In *Proceedings of the AAAI Conference on Artificial Intelligence*, volume 33, pages 7801–7808.
- Chiappa, S. and Pacchiano, A. (2021). Fairness with continuous optimal transport. *arXiv preprint arXiv:2101.02084*.
- Çınlar, E. and Çınlar, E. (2011). *Probability and stochastics*, volume 261. Springer.
- Cohen, T. and Welling, M. (2016). Group equivariant convolutional networks. In *International conference on machine learning*, pages 2990–2999. PMLR.
- Dinculeanu, N. (2000). *Vector integration and stochastic integration in Banach spaces*, volume 48. John Wiley & Sons.
- Fukumizu, K., Gretton, A., Sun, X., and Schölkopf, B. (2007). Kernel measures of conditional dependence. In *Advances in neural information processing systems*, volume 20.
- Fukumizu, K., Song, L., and Gretton, A. (2013). Kernel bayes’ rule: Bayesian inference with positive definite kernels. *Journal of Machine Learning Research*, 14(1):3753–3783.
- Grünewälder, S., Lever, G., Gretton, A., Baldassarre, L., Patterson, S., and Pontil, M. (2012). Conditional mean embeddings as regressors. In *International conference on machine learning*.
- Hardt, M., Price, E., Price, E., and Srebro, N. (2016). Equality of opportunity in supervised learning. In *Advances in Neural Information Processing Systems*, volume 29.
- Heinze-Deml, C., Peters, J., and Meinshausen, N. (2018). Invariant causal prediction for nonlinear models. *Journal of Causal Inference*, 6(2).
- Kilbertus, N., Rojas Carulla, M., Parascandolo, G., Hardt, M., Janzing, D., and Schölkopf, B. (2017). Avoiding discrimination through causal reasoning. In *Advances in neural information processing systems*, volume 30.
- Kingma, D. P. and Welling, M. (2014). Auto-encoding variational bayes. In *2nd International Conference on Learning Representations, ICLR 2014*.
- Kohavi, R. and Becker, B. (1996). Uci adult data set. *UCI Machine Learning Repository*.
- Krizhevsky, A., Sutskever, I., and Hinton, G. E. (2012). Imagenet classification with deep convolutional neural networks. In *Advances in Neural Information Processing Systems*, volume 25.
- Kusner, M. J., Loftus, J. R., Russell, C., and Silva, R. (2017). Counterfactual fairness. In *Advances in Neural Information Processing Systems*, pages 4066–4076.
- Lu, C., Wu, Y., Hernández-Lobato, J. M., and Schölkopf, B. (2021). Invariant causal representation learning for out-of-distribution generalization. In *International Conference on Learning Representations*.
- Mary, J., Calauzènes, C., and Karoui, N. E. (2019). Fairness-aware learning for continuous attributes and treatments. In *International Conference on Machine Learning*, volume 97, pages 4382–4391. PMLR.

- Matthey, L., Higgins, I., Hassabis, D., and Lerchner, A. (2017). dsprites: Disentanglement testing sprites dataset. <https://github.com/deepmind/dsprites-dataset/>.
- Mitchell, S., Potash, E., Barocas, S., D’Amour, A., and Lum, K. (2021). Algorithmic fairness: Choices, assumptions, and definitions. *Annual Review of Statistics and Its Application*, 8:141–163.
- Muandet, K., Fukumizu, K., Sriperumbudur, B., and Schölkopf, B. (2017). Kernel mean embedding of distributions: A review and beyond. *Foundations and Trends in Machine Learning*, 10(1-2):1–141.
- Nabi, R. and Shpitser, I. (2018). Fair inference on outcomes. In *Proceedings of the AAAI Conference on Artificial Intelligence*, volume 32.
- Park, J. and Muandet, K. (2020). A measure-theoretic approach to kernel conditional mean embeddings. In *Advances in Neural Information Processing Systems*, pages 21247–21259.
- Pearl, J. (2000). *Causality: Models, Reasoning and Inference*. Cambridge University Press.
- Peters, J., Bühlmann, P., and Meinshausen, N. (2016). Causal inference by using invariant prediction: identification and confidence intervals. *Journal of the Royal Statistical Society: Series B (Statistical Methodology)*, 78(5):947–1012.
- Rahimi, A. and Recht, B. (2007). Random features for large-scale kernel machines. In *Advances in Neural Information Processing Systems*, pages 1177–1184.
- Rojas-Carulla, M., Schölkopf, B., Turner, R., and Peters, J. (2018). Invariant models for causal transfer learning. *The Journal of Machine Learning Research*, 19(1):1309–1342.
- Schölkopf, B., Smola, A. J., Bach, F., et al. (2002). *Learning with kernels: support vector machines, regularization, optimization, and beyond*. MIT press.
- Shorten, C. and Khoshgoftaar, T. M. (2019). A survey on image data augmentation for deep learning. *Journal of big data*, 6(1):1–48.
- Shpitser, I. and Pearl, J. (2006). Identification of joint interventional distributions in recursive semi-markovian causal models. In *Proceedings of the AAAI Conference on Artificial Intelligence*, pages 1219–1226.
- Shpitser, I. and Pearl, J. (2008). Complete identification methods for the causal hierarchy. *Journal of Machine Learning Research*, 9:1941–1979.
- Shpitser, I. and Pearl, J. (2009). Effects of treatment on the treated: Identification and generalization. In *Proceedings of the Twenty-Fifth Conference on Uncertainty in Artificial Intelligence*, pages 514–521.
- Smola, A., Gretton, A., Song, L., and Schölkopf, B. (2007). A hilbert space embedding for distributions. In *International Conference on Algorithmic Learning Theory*, pages 13–31. Springer.
- Song, L., Fukumizu, K., and Gretton, A. (2013). Kernel embeddings of conditional distributions: A unified kernel framework for nonparametric inference in graphical models. *IEEE Signal Processing Magazine*, 30(4):98–111.
- Song, L., Huang, J., Smola, A. J., and Fukumizu, K. (2009). Hilbert space embeddings of conditional distributions with applications to dynamical systems. In *International Conference on Machine Learning*, volume 382, pages 961–968.
- Szabó, Z. and Sriperumbudur, B. K. (2017). Characteristic and universal tensor product kernels. *Journal of Machine Learning Research*, 18:233:1–233:29.



- Vaswani, A., Shazeer, N., Parmar, N., Uszkoreit, J., Jones, L., Gomez, A. N., Kaiser, Ł., and Polosukhin, I. (2017). Attention is all you need. In *Advances in Neural Information Processing Systems*, volume 30.
- Veitch, V., D’Amour, A., Yadlowsky, S., and Eisenstein, J. (2021). Counterfactual invariance to spurious correlations in text classification. In *Advances in Neural Information Processing Systems*, pages 16196–16208.
- Xie, Q., Dai, Z., Hovy, E., Luong, T., and Le, Q. (2020). Unsupervised data augmentation for consistency training. In *Advances in Neural Information Processing Systems*, volume 33, pages 6256–6268.
- Zaheer, M., Kottur, S., Ravanbakhsh, S., Poczos, B., Salakhutdinov, R. R., and Smola, A. J. (2017). Deep sets. In *Advances in Neural Information Processing Systems*, volume 30.

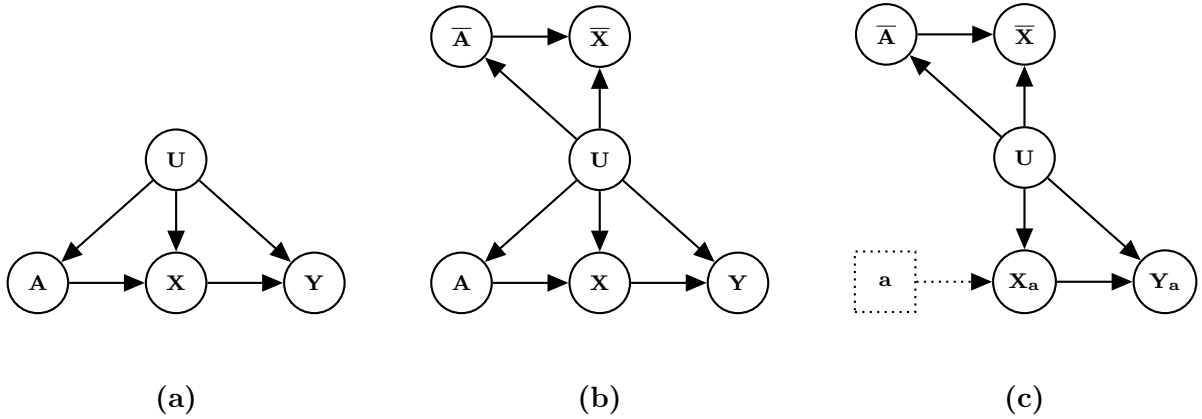


Figure 7: (a) **A causal graph**  $\mathcal{G}$ , which embeds information for the random variables of the model in the pre-interventional world. (b) **The corresponding graph**  $\mathcal{G}'$  for the set  $\mathbf{W} = \{\mathbf{A}, \mathbf{X}\}$ . The variables  $\bar{\mathbf{A}}$  and  $\bar{\mathbf{X}}$  are *copies* of  $\mathbf{A}$  and  $\mathbf{X}$  respectively. (c) **The post-interventional graph**  $\mathcal{G}'_a$ . By construction, any intervention of the form  $\mathbf{A} \leftarrow \mathbf{a}$  does not affect the group  $\bar{\mathbf{W}} = \{\bar{\mathbf{A}}, \bar{\mathbf{X}}\}$ .

## Appendix

### A Missing proof of Theorem 3.2

In this section, we give proof of Theorem 3.2, which we restate for completeness.

#### A.1 Overview of the proof techniques

**Theorem 3.2.** *Let  $\mathcal{G}$  be a causal diagram, and consider two (not necessarily disjoint) sets of nodes  $\mathbf{A}$ ,  $\mathbf{W}$ . Let  $\mathbf{Z}$  be a set of nodes that blocks all non-directed paths from  $\mathbf{A} \cup \mathbf{W}$  to  $\mathbf{Y}$ . Then, for any SCM compatible with  $\mathcal{G}$ , any predictor  $\hat{\mathbf{Y}}$  that satisfies  $\hat{\mathbf{Y}} \perp\!\!\!\perp \mathbf{A} \mid \mathbf{Z}$  is counterfactually invariant in  $\mathbf{A}$  with respect to  $\mathbf{W}$ .*

Our proof technique generalizes the work of Shpitser and Pearl [2009]. To understand the proof technique, note that conditional counterfactual distributions of the form  $\mathbb{P}_{\mathbf{Y}_a^* | \mathbf{W}}(\mathbf{y} \mid \mathbf{w})$  involve quantities *from two different worlds*. The variables  $\mathbf{W}$  belong to the pre-interventional world, and the interventional variable  $\mathbf{Y}_a^*$  belongs to the world after performing the intervention  $\mathbf{A} \leftarrow \mathbf{a}$ . Hence, we study the identification of conditional counterfactual distributions using a diagram that embeds the causal relationships between the pre- and the post-interventional world. After defining this diagram, we prove that some conditional measures in this new model provide an estimate for  $\mathbb{P}_{\mathbf{Y}_a^* | \mathbf{W}}(\mathbf{y} \mid \mathbf{w})$ . We then combine this result with the properties of  $\mathbf{Z}$  to prove the desired result.

#### A.2 A graphical criterion for conditional independence

In this section, we discuss a well-known criterion for conditional independence, which we will then use to prove Theorem 3.2. To this end, we use the notion of a blocked path, which we restate for clarity.

**Definition 3.1.** Consider a path  $\pi$  of causal graph  $\mathcal{G}$ . A set of nodes  $\mathbf{Z}$  blocks  $\pi$ , if  $\pi$  contains a triple of consecutive nodes connected in one of the following ways:  $N_i \rightarrow Z \rightarrow N_j$ ,  $N_i \leftarrow Z \rightarrow N_j$ , or  $N_i \rightarrow M \leftarrow N_j$ , with  $N_i, N_j \notin \mathbf{Z}$ ,  $Z \in \mathbf{Z}$ , and neither  $M$  nor any descendent of  $M$  is in  $\mathbf{Z}$ .

Using Definition A.1, we define the concept of  $d$ -separation as follows.

**Definition A.1** ( $d$ -Separation). Consider a causal graph  $\mathcal{G}$ . Two sets of nodes  $\mathbf{X}$  and  $\mathbf{Y}$  of  $\mathcal{G}$

are said to be  $d$ -separated by a third set  $\mathbf{Z}$  if every path from any node of  $\mathbf{X}$  to any node of  $\mathbf{Y}$  is blocked by  $\mathbf{Z}$ .

Definition A.1 is a graphical criterion for conditional independence. In fact, the following well-known result holds [Pearl, 2000].

**Lemma A.2** ( $d$ -Separation Criterion). *Consider a causal graph  $\mathcal{G}$ , and suppose that two sets of nodes  $\mathbf{X}$  and  $\mathbf{Y}$  of  $\mathcal{G}$  are  $d$ -separated by  $\mathbf{Z}$ . Then,  $\mathbf{X}$  is independent of  $\mathbf{Y}$  given  $\mathbf{Z}$  in any model induced by the graph  $\mathcal{G}$ .*

We use the notation  $\mathbf{X} \perp\!\!\!\perp_{\mathcal{G}} \mathbf{Y} \mid \mathbf{Z}$  to indicate that  $\mathbf{X}$  and  $\mathbf{Y}$  are  $d$ -separated by  $\mathbf{U}$  in  $\mathcal{G}$ .

### A.3 Identifiability of conditional counterfactual distributions

A natural way to study the relationships between the pre- and the post-interventional world is to use the counterfactual graph [Shpitser and Pearl, 2008]. However, the construction of the counterfactual graph is rather intricate. For our purposes it is sufficient to consider a simpler construction. Consider an SGM with causal graph  $\mathcal{G}$ , and fix a set of observable random variables  $\mathbf{W}$ . We define the corresponding graph  $\mathcal{G}'$  in the following three steps:

1. define  $\mathcal{G}'$  to be the same graph as  $\mathcal{G}$ ;
2. add a new node  $\overline{W}$  to  $\mathcal{G}'$ , for each node  $W$  of the set  $\mathbf{W}$ ;
3. for each node  $W$  of the set  $\mathbf{W}$  and for each parent  $W'$  of  $W$ , if  $W' \in \mathbf{W}$  then add an edge  $\overline{W} \rightarrow \overline{W}'$  to  $\mathcal{G}'$ ; if  $W' \notin \mathbf{W}$  add an edge  $W' \rightarrow \overline{W}$  to  $\mathcal{G}'$ .

An illustration of this graph is presented in Figure 7. Note that any node  $\overline{W}$  defined as above does not have any descendants in  $\mathcal{G}'$ . In the remainder of this section, we denote with  $\overline{\mathbf{W}}$  the set of all nodes  $\overline{W}$  in  $\mathcal{G}'$  defined as above. We remark that this construction generalizes the work by Shpitser and Pearl [2009].

Fix a second set  $\mathbf{A}$  of nodes of  $\mathcal{G}$ , and consider interventions of the form  $\mathbf{A} \leftarrow \mathbf{a}$ , as in the statement of Theorem 3.2. We prove that any conditional counterfactual distribution of the form  $\mathbb{P}_{\mathbf{Y}_{\mathbf{a}}^* | \mathbf{W}}(\mathbf{y} \mid \mathbf{w})$  are identifiable in  $\mathcal{G}$  if and only if the corresponding probability distributions  $\mathbb{P}_{\mathbf{Y} | \overline{\mathbf{W}}}(\mathbf{y} \mid \overline{\mathbf{w}})$  are identifiable in  $\mathcal{G}'_{\mathbf{a}}$ . The following theorem generalizes Theorem 1 by Shpitser and Pearl [2009].

**Theorem A.3.** *Let  $\mathcal{G}$  be a causal diagram, and consider two sets of nodes  $\mathbf{A}$ ,  $\mathbf{W}$  (not necessarily disjoint). Consider the corresponding graph  $\mathcal{G}'$  as defined above. If the distribution  $\mathbb{P}_{\mathbf{Y}_{\mathbf{a}}^* | \mathbf{W}}(\mathbf{y} \mid \mathbf{w})$  is identifiable in  $\mathcal{G}$ , then the distribution  $\mathbb{P}_{\mathbf{Y} | \overline{\mathbf{W}}}(\mathbf{y} \mid \overline{\mathbf{w}})$  is identifiable in  $\mathcal{G}'_{\mathbf{a}}$ , for any model induced by  $\mathcal{G}$ . Furthermore, the estimand  $\mathbb{P}_{\mathbf{Y} | \overline{\mathbf{W}}}(\mathbf{y} \mid \mathbf{w})$  in  $\mathcal{G}'_{\mathbf{a}}$  is correct for  $\mathbb{P}_{\mathbf{Y}_{\mathbf{a}}^* | \mathbf{W}}(\mathbf{y} \mid \mathbf{w})$ .*

To prove Theorem A.3, we introduce additional concepts. We first introduce the notion of a  $C$ -forest and the notion of an edge [Shpitser and Pearl, 2006].

**Definition A.4** ( $C$ -Forest). Let  $\mathcal{G}$  be a causal diagram, and consider a complete sub-graph  $\mathcal{H}$  of  $\mathcal{G}$ . Denote with  $\mathbf{R}$  the maximal root set of  $\mathcal{H}$ . We say that  $\mathcal{H}$  is a  $\mathbf{R}$ -rooted  $C$ -forest if a subset of its bi-directed arcs forms a spanning tree over all vertices in  $\mathcal{H}$ , and all the observable nodes of  $\mathcal{H}$  have at most one child.

In our analysis we also use the following definition.

**Definition A.5** (Edge). Let  $\mathcal{G}$  be a causal diagram, and fix a set of nodes  $\mathbf{A}$ . Consider two  $\mathbf{R}$ -rooted  $C$ -forests  $\mathcal{H}$ ,  $\mathcal{K}$  of  $\mathcal{G}$  such that (i)  $\mathcal{H}$  is a sub-graph of  $\mathcal{K}$ ; (ii)  $\mathcal{H}$  and  $\mathcal{K}$  do not contain any variable in  $\mathbf{A}$ ; (iii) the nodes of  $\mathbf{R}$  are ancestors of  $\mathbf{Y}$  in the graph  $\mathcal{G}_{\mathbf{a}}$ . Then, we say that  $\mathcal{H}$  and  $\mathcal{K}$  form an edge for  $\mathbb{P}_{\mathbf{Y}_{\mathbf{a}}^*}(\mathbf{y})$  in  $\mathcal{G}$ .

There is a connection between these concepts and the identifiability of counterfactual distributions, as shown in the following theorem.

**Theorem A.6** (Theorem 4 by Shpitser and Pearl [2006]). *Let  $\mathcal{G}$  be a causal diagram, and fix a set of nodes  $\mathbf{A}$ . Suppose that there exist two sub-graphs of  $\mathcal{G}$  that form an edge for  $\mathbb{P}_{\mathbf{Y}_{\mathbf{a}}^*}(\mathbf{y})$ . Then,  $\mathbb{P}_{\mathbf{Y}_{\mathbf{a}}^*}(\mathbf{y})$  is not identifiable in  $\mathcal{G}$ .*

Using these concepts, we can prove Theorem A.3.

*Proof of Theorem A.3.* For simplicity, denote with  $\mathbb{P}^*$  the induced measure on  $\mathcal{G}'_{\mathbf{a}}$ . We first prove that  $\mathbb{P}_{\mathbf{Y}_{\mathbf{a}}^*|\mathbf{W}}(\mathbf{y} | \mathbf{w})$  is identifiable in  $\mathcal{G}$  if and only if  $\mathbb{P}_{\mathbf{Y}|\overline{\mathbf{W}}}^*(\mathbf{y} | \overline{\mathbf{w}})$  is identifiable in  $\mathcal{G}'_{\mathbf{a}}$ . We distinguish two cases, based on whether  $\overline{\mathbf{W}}$  is  $d$ -separated from  $\mathbf{Y}$  in  $\mathcal{G}'_{\mathbf{a}}$  or not.

**Case 1:  $\overline{\mathbf{W}}$  is  $d$ -separated from  $\mathbf{Y}$  in  $\mathcal{G}'_{\mathbf{a}}$ .** By Lemma A.2 we have that  $\mathbf{Y}$  is independent of  $\overline{\mathbf{W}}$ . Hence,  $\mathbb{P}_{\mathbf{Y}|\overline{\mathbf{W}}}^*(\mathbf{y} | \overline{\mathbf{w}})$  is identifiable if and only if

$$\mathbb{P}_{\mathbf{Y}|\overline{\mathbf{W}}}^*(\mathbf{y} | \overline{\mathbf{w}}) = \mathbb{P}_{\mathbf{Y}}^*(\mathbf{y}) = \mathbb{P}_{\mathbf{Y}_{\mathbf{a}}^*}(\mathbf{y}) \quad (5)$$

is identifiable in  $\mathcal{G}'_{\mathbf{a}}$ . Suppose that  $\mathbb{P}_{\mathbf{Y}_{\mathbf{a}}^*|\mathbf{W}}(\mathbf{y} | \mathbf{w})$  is not identifiable. Then,  $\mathbb{P}_{\mathbf{Y}_{\mathbf{a}}^*}(\mathbf{y})$  is not identifiable, and  $\mathbb{P}_{\mathbf{Y}|\overline{\mathbf{W}}}^*(\mathbf{y} | \overline{\mathbf{w}})$  is also not identifiable by eq. (5).

**Case 2:  $\overline{\mathbf{W}}$  is not  $d$ -separated from  $\mathbf{Y}$  in  $\mathcal{G}'_{\mathbf{a}}$ .** Assume without loss of generality that any variable of  $\mathbf{A} \cup \mathbf{W}$  is not a descendent of  $\mathbf{Y}$  in  $\mathcal{G}$  (otherwise it has no effect on  $\mathbf{Y}$ ). Under this assumption, there exists a set of random variables  $\overline{\mathbf{U}} \subseteq \overline{\mathbf{W}}$  such that there exists an edge for  $\mathbb{P}_{(\mathbf{Y} \cup \overline{\mathbf{U}})_{\mathbf{a}}^*}(\mathbf{y}, \overline{\mathbf{u}}) = \mathbb{P}_{\mathbf{Y}, \overline{\mathbf{U}}}^*(\mathbf{y}, \overline{\mathbf{u}})$  in  $\mathcal{G}'$ . It follows that  $\mathbb{P}_{\mathbf{Y}, \overline{\mathbf{U}}}^*(\mathbf{y}, \overline{\mathbf{u}})$  is not identifiable. Since  $\overline{\mathbf{U}} \subseteq \overline{\mathbf{W}}$ , it follows that the distribution  $\mathbb{P}_{\mathbf{Y}, \overline{\mathbf{W}}}^*(\mathbf{y}, \overline{\mathbf{w}})$  is also not identifiable.

We conclude by showing that the estimand expression is correct. To this end, note that since  $\mathcal{G}'$  is just a causal diagram, the estimand of the post-interventional distribution  $\mathbb{P}_{\mathbf{Y}|\overline{\mathbf{W}}}^*(\mathbf{y} | \overline{\mathbf{w}})$  is correct for  $\mathbb{P}_{\mathbf{Y}_{\mathbf{a}, \mathbf{x}}^*|\mathbf{A}, \mathbf{X}}(\mathbf{y} | \mathbf{a}', \mathbf{x})$ . Since the set  $\overline{\mathbf{W}}$  only contains variable copies of  $\mathbf{A} \cup \mathbf{X}$ , as claimed.  $\square$

## A.4 Valid adjustments for conditional interventional distributions

Here we discuss a criterion for the identification of conditional distributions, which we will then use to prove Theorem 3.2. We follow Pearl [2000] to this end, and use the  $d$ -separation criterion to define valid adjustment sets for conditional counterfactual distributions.

Consider a model with causal graph  $\mathcal{G}$ , and fix a set of observed variables  $\mathbf{A}$ . We define an auxiliary graph  $\mathcal{G}_{\mathbf{I}}$ , by adding to  $\mathcal{G}$  an additional node  $\mathbf{I}$ . This node is a parent of the nodes in the set  $\mathbf{A}$ , and it has no other neighbour. We modify the structural assignments of the nodes  $\mathbf{A}$ , so that for  $\mathbf{I} = 0$  the values of  $\mathbf{A}$  are determined as in  $\mathcal{G}$ , whereas for  $\mathbf{I} = 1$  the values of  $\mathbf{A}$  are set to  $\mathbf{A} = \mathbf{a}$ . The node  $\mathbf{I}$  corresponds to a Bernoulli distribution, with  $\mathbf{I} = 1$  indicating that the intervention took place. This construction is important, because the following lemma holds.

**Lemma A.7.** *Consider an SGM  $\mathcal{G}$  and fix two disjoint groups of observed variables  $\mathbf{X}$  and  $\mathbf{Y}$ . Denote with  $\mathcal{G}_{\mathbf{I}}$  the auxiliary graph as defined above, with respect to an intervention  $\mathbf{A} \leftarrow \mathbf{a}$ . Let  $\mathbf{Z}$  a set of nodes of  $\mathcal{G}$  such that  $\mathbf{Y} \perp_{\mathcal{G}_{\mathbf{I}}} \mathbf{I} | \mathbf{A}, \mathbf{Z}$ . Then, it holds*

$$\mathbb{P}_{\mathbf{Y}|\mathbf{Z}}^*(\mathbf{y} | \mathbf{z}) = \mathbb{P}_{\mathbf{Y}|\mathbf{A}, \mathbf{Z}}(\mathbf{y} | \mathbf{a}, \mathbf{z}).$$

Here,  $\mathbb{P}^*$  the post-interventional distribution, after assigning  $\mathbf{A} \leftarrow \mathbf{a}$ .

*Proof.* It holds

$$\begin{aligned} \mathbb{P}_{\mathbf{Y}|\mathbf{Z}}^*(\mathbf{y} | \mathbf{z}) &= \mathbb{P}_{\mathbf{Y}|\mathbf{A}, \mathbf{Z}}^*(\mathbf{y} | \mathbf{a}, \mathbf{z}) && \text{(by definition of } \mathbb{P}^*) \\ &= \mathbb{P}_{\mathbf{Y}|\mathbf{I}, \mathbf{A}, \mathbf{Z}}(\mathbf{y} | \mathbf{i} = 1, \mathbf{a}, \mathbf{z}) && \text{(by the definition of } \mathbf{I}) \\ &= \mathbb{P}_{\mathbf{Y}|\mathbf{I}, \mathbf{A}, \mathbf{Z}}(\mathbf{y} | \mathbf{i} = 0, \mathbf{a}, \mathbf{z}) && \text{(by Lemma A.2)} \\ &= \mathbb{P}_{\mathbf{Y}|\mathbf{A}, \mathbf{Z}}(\mathbf{y} | \mathbf{a}, \mathbf{z}), && \text{(by the definition of } \mathbf{I}) \end{aligned}$$

as claimed.  $\square$

The following lemma characterizes all sets  $\mathbf{Z}$  that fulfills the condition as in Lemma A.7.

**Lemma A.8.** *Consider an SGM  $\mathcal{G}$ , and denote with  $\mathcal{G}_{\mathbf{I}}$  the auxiliary graph as defined above, with respect to an intervention  $\mathbf{A} \leftarrow \mathbf{a}$ . Let  $\mathbf{Z}$  a set of nodes that blocks all non-directed paths from  $\mathbf{A}$  to  $\mathbf{Y}$ . Then, it holds  $\mathbf{Y} \perp\!\!\!\perp_{\mathcal{G}_{\mathbf{I}}} \mathbf{I} \mid \mathbf{A}, \mathbf{Z}$ . In particular, it holds  $\mathbb{P}_{\mathbf{Y}|\mathbf{Z}}^*(\mathbf{y} \mid \mathbf{z}) = \mathbb{P}_{\mathbf{Y}|\mathbf{A},\mathbf{Z}}(\mathbf{y} \mid \mathbf{a}, \mathbf{z})$ .*

*Proof.* Denote with  $\pi$  any path from  $\mathbf{I}$  to  $\mathbf{Y}$  in  $\mathcal{G}_{\mathbf{I}}$ . Since  $\mathbf{I}$  is a parent of every node in  $\mathbf{A}$ , and since  $\mathbf{I}$  has no parents, then any path  $\pi$  can be decomposed into two paths  $\pi_1, \pi_2$ , where  $\pi_1$  is a single edge from  $\mathbf{I}$  to  $\mathbf{A}$ , and  $\pi_2$  is a path from  $\mathbf{A}$  to  $\mathbf{Y}$ . If  $\pi$  is a causal path, then  $\mathbf{A}$  acts as a separator for this path. If  $\pi$  is not a causal path from  $\mathbf{I}$  to  $\mathbf{Y}$ , then it must be undirected (since  $\mathbf{I}$  has no parents). It follows that  $\pi_2$  is an undirected path from  $\mathbf{A}$  to  $\mathbf{Y}$ , which is  $d$ -separated by  $\mathbf{Z}$ . Hence,  $\pi$  is  $d$ -separated. We conclude that  $\mathbf{Y} \perp\!\!\!\perp_{\mathcal{G}_{\mathbf{I}}} \mathbf{I} \mid \mathbf{A}, \mathbf{Z}$ . The second part of the claim follows by Lemma A.7.  $\square$

## A.5 Proof of Theorem 3.2

Theorem A.3 tells us that we can identify conditional counterfactual distributions in  $\mathcal{G}$ , by identifying distributions on  $\mathcal{G}'$ . We can combine this observation with the notion of a valid adjustment set to derive a closed formula for the identification of the distributions of interest.

*Proof of Theorem 3.2.* Let  $\mathcal{G}'$  be the augmented graph obtained by adding nodes  $\overline{\mathbf{W}}$  to  $\mathcal{G}$ , as described in Section A.3. Denote with  $\mathbb{P}^*$  the induced measure on  $\mathcal{G}'_{\mathbf{a}}$ . Suppose that it holds

$$\mathbb{P}_{\mathbf{Y}_{\mathbf{a}}|\mathbf{W}}(\mathbf{y} \mid \mathbf{w}) = \int \mathbb{P}_{\mathbf{Y}|\mathbf{A},\mathbf{Z}}(\mathbf{y} \mid \mathbf{a}, \mathbf{z}) d\mathbb{P}_{\mathbf{Z}|\overline{\mathbf{W}}}^*(\mathbf{z} \mid \mathbf{w}) \quad (6)$$

for any intervention  $\mathbf{A} \leftarrow \mathbf{a}$ , and for any possible value  $\mathbf{w}$  attained by  $\mathbf{W}$ . Then the claim follows. In fact, assuming that eq. (6) holds, we have that

$$\begin{aligned} \mathbb{P}_{\mathbf{Y}_{\mathbf{a}}|\mathbf{W}}(\mathbf{y} \mid \mathbf{w}) &= \int \mathbb{P}_{\mathbf{Y}|\mathbf{A},\mathbf{Z}}(\mathbf{y} \mid \mathbf{a}, \mathbf{z}) d\mathbb{P}_{\mathbf{Z}|\overline{\mathbf{W}}}^*(\mathbf{z} \mid \mathbf{w}) && \text{(assuming eq. (6))} \\ &= \int \mathbb{P}_{\mathbf{Y}|\mathbf{A},\mathbf{Z}}(\mathbf{y} \mid \mathbf{a}', \mathbf{z}) d\mathbb{P}_{\mathbf{Z}|\overline{\mathbf{W}}}^*(\mathbf{z} \mid \mathbf{w}) && \text{(since } \mathbf{Y} \perp\!\!\!\perp \mathbf{A} \mid \mathbf{Z}) \\ &= \mathbb{P}_{\mathbf{Y}_{\mathbf{a}'}}(\mathbf{y} \mid \mathbf{w}). && \text{(assuming eq. (6))} \end{aligned}$$

Hence, the proof of Theorem 3.2 boils down to proving eq. (6). To this end, since  $\mathbf{Z}$  breaks all non-directed paths from  $\mathbf{W}$  to  $\mathbf{Y}$ , then by construction  $\mathbf{Z}$  is a  $d$ -separator between  $\overline{\mathbf{W}}$  and  $\mathbf{Y}$  in the post-interventional graph  $\mathcal{G}'_{\mathbf{a}}$ . Hence, it holds

$$\begin{aligned} \mathbb{P}_{\mathbf{Y},\overline{\mathbf{W}}}^*(\mathbf{y}, \mathbf{w}) &= \int \mathbb{P}_{\mathbf{Y}|\overline{\mathbf{W}},\mathbf{Z}}^*(\mathbf{y} \mid \mathbf{w}, \mathbf{z}) d\mathbb{P}_{\overline{\mathbf{W}},\mathbf{Z}}^*(\mathbf{w}, \mathbf{z}) && \text{(by conditioning)} \\ &= \int \mathbb{P}_{\mathbf{Y}|\mathbf{Z}}^*(\mathbf{y} \mid \mathbf{z}) d\mathbb{P}_{\overline{\mathbf{W}},\mathbf{Z}}^*(\mathbf{w}, \mathbf{z}) && \text{(since } \mathbf{Y} \perp\!\!\!\perp_{\mathcal{G}'_{\mathbf{a}}} \overline{\mathbf{W}} \mid \mathbf{Z}) \\ &= \int \mathbb{P}_{\mathbf{Y}|\mathbf{A},\mathbf{Z}}(\mathbf{y} \mid \mathbf{a}, \mathbf{z}) d\mathbb{P}_{\overline{\mathbf{W}},\mathbf{Z}}^*(\mathbf{w}, \mathbf{z}). && \text{(by Lemma A.7)} \end{aligned}$$

By the standard property of conditional distributions, we conclude that

$$\mathbb{P}_{\mathbf{Y}|\overline{\mathbf{W}}}^*(\mathbf{y} \mid \mathbf{w}) = \int \mathbb{P}_{\mathbf{Y}|\mathbf{A},\mathbf{Z}}(\mathbf{y} \mid \mathbf{a}, \mathbf{z}) d\mathbb{P}_{\mathbf{Z}|\overline{\mathbf{W}}}^*(\mathbf{z} \mid \mathbf{w}).$$

The claim follows by applying Theorem A.3 to the equation above, since it holds  $\mathbb{P}_{\mathbf{Y}|\overline{\mathbf{W}}}^*(\mathbf{y} \mid \mathbf{w}) = \mathbb{P}_{\mathbf{Y}_{\mathbf{a}}|\mathbf{W}}(\mathbf{y} \mid \mathbf{w})$ .  $\square$



## B Missing proof of Theorem 3.4

We prove that the HSCIC can be used to promote conditional independence, using a similar technique as [Park and Muandet \[2020\]](#). The following theorem holds.

**Theorem 3.4.** *With the notation introduced above, suppose that the kernel  $k$  of the tensor product space  $\mathcal{H}_{\mathbf{X}} \otimes \mathcal{H}_{\mathbf{A}}$  is characteristic.<sup>3</sup> Then,  $\text{HSCIC}(\mathbf{Y}, \mathbf{A} \mid \mathbf{Z}) = 0$  almost surely if and only if  $\mathbf{Y} \perp\!\!\!\perp \mathbf{A} \mid \mathbf{Z}$ .*

*Proof.* By definition, we can write  $\text{HSCIC}(\mathbf{Y}, \mathbf{A} \mid \mathbf{Z}) = H_{\mathbf{Y}, \mathbf{A} \mid \mathbf{Z}} \circ \mathbf{Z}$ , where  $H_{\mathbf{Y}, \mathbf{A} \mid \mathbf{Z}}$  is a real-valued deterministic function. Hence, the HSCIC is a real-valued random variable, defined over the same domain  $\Omega_{\mathbf{Z}}$  of the random variable  $\mathbf{X}$ .

We first prove that if  $\text{HSCIC}(\mathbf{Y}, \mathbf{A} \mid \mathbf{Z}) = 0$  almost surely, then it holds  $\mathbf{Y} \perp\!\!\!\perp \mathbf{A} \mid \mathbf{Z}$ . To this end, consider an event  $\Omega' \subseteq \Omega_{\mathbf{X}}$  that occurs almost surely, and such that it holds  $(H_{\mathbf{Y}, \mathbf{A} \mid \mathbf{X}} \circ \mathbf{X})(\omega) = 0$  for all  $\omega \in \Omega'$ . Fix a sample  $\omega \in \Omega'$ , and consider the corresponding value  $\mathbf{z}_\omega = \mathbf{Z}(\omega)$ , in the support of  $\mathbf{Z}$ . It holds

$$\begin{aligned}
 \int k(\mathbf{y} \otimes \mathbf{a}, \cdot) d\mathbb{P}_{\mathbf{Y}, \mathbf{A} \mid \mathbf{Z}=\mathbf{z}_\omega} &= \mu_{\mathbf{Y}, \mathbf{A} \mid \mathbf{Z}=\mathbf{z}_\omega} && \text{(by definition)} \\
 &= \mu_{\mathbf{Y} \mid \mathbf{Z}=\mathbf{z}_\omega} \otimes \mu_{\mathbf{A} \mid \mathbf{Z}=\mathbf{z}_\omega} && \text{(since } \omega \in \Omega') \\
 &= \int k_{\mathbf{Y}}(\mathbf{y}, \cdot) d\mathbb{P}_{\mathbf{Y} \mid \mathbf{Z}=\mathbf{z}_\omega} \otimes \int k_{\mathbf{A}}(\mathbf{a}, \cdot) d\mathbb{P}_{\mathbf{A} \mid \mathbf{Z}=\mathbf{z}_\omega} && \text{(by definition)} \\
 &= \int k_{\mathbf{Y}}(\mathbf{y}, \cdot) \otimes k_{\mathbf{A}}(\mathbf{a}, \cdot) d\mathbb{P}_{\mathbf{Y} \mid \mathbf{Z}=\mathbf{z}_\omega} \mathbb{P}_{\mathbf{A} \mid \mathbf{Z}=\mathbf{z}_\omega}, && \text{(by Fubini's Theorem)}
 \end{aligned}$$

with  $k_{\mathbf{Y}}$  and  $k_{\mathbf{A}}$  the kernels of  $\mathcal{H}_{\mathbf{Y}}$  and  $\mathcal{H}_{\mathbf{A}}$  respectively. Since the kernel  $k$  of the tensor product space  $\mathcal{H}_{\mathbf{Y}} \otimes \mathcal{H}_{\mathbf{A}}$  is characteristic, then the kernels  $k_{\mathbf{Y}}$  and  $k_{\mathbf{A}}$  are also characteristic. Hence, it holds  $\mathbb{P}_{\mathbf{Y}, \mathbf{A} \mid \mathbf{Z}=\mathbf{z}_\omega} = \mathbb{P}_{\mathbf{Y} \mid \mathbf{Z}=\mathbf{z}_\omega} \mathbb{P}_{\mathbf{A} \mid \mathbf{Z}=\mathbf{z}_\omega}$  for all  $\omega \in \Omega'$ . Since the event  $\Omega'$  occurs almost surely, then  $\mathbb{P}_{\mathbf{Y}, \mathbf{A} \mid \mathbf{Z}=\mathbf{z}_\omega} = \mathbb{P}_{\mathbf{Y} \mid \mathbf{Z}=\mathbf{z}_\omega} \mathbb{P}_{\mathbf{A} \mid \mathbf{Z}=\mathbf{z}_\omega}$  almost surely, that is  $\mathbf{Y} \perp\!\!\!\perp \mathbf{A} \mid \mathbf{Z}$ .

Assume now that  $\mathbf{Y} \perp\!\!\!\perp \mathbf{A} \mid \mathbf{Z}$ . By definition there exists an event  $\Omega'' \subseteq \Omega_{\mathbf{Z}}$  such that  $\mathbb{P}_{\mathbf{Y}, \mathbf{A} \mid \mathbf{Z}=\mathbf{z}_\omega} = \mathbb{P}_{\mathbf{Y} \mid \mathbf{Z}=\mathbf{z}_\omega} \mathbb{P}_{\mathbf{A} \mid \mathbf{Z}=\mathbf{z}_\omega}$  for all samples  $\omega \in \Omega''$ , with  $\mathbf{z}_\omega = \mathbf{Z}(\omega)$ . It holds

$$\begin{aligned}
 \mu_{\mathbf{Y}, \mathbf{A} \mid \mathbf{Z}=\mathbf{z}_\omega} &= \int k(\mathbf{y} \otimes \mathbf{a}, \cdot) d\mathbb{P}_{\mathbf{Y}, \mathbf{A} \mid \mathbf{Z}=\mathbf{z}_\omega} && \text{(by definition)} \\
 &= \int k(\mathbf{y} \otimes \mathbf{a}, \cdot) d\mathbb{P}_{\mathbf{Y} \mid \mathbf{Z}=\mathbf{z}_\omega} \mathbb{P}_{\mathbf{A} \mid \mathbf{Z}=\mathbf{z}_\omega} && \text{(since } \omega \in \Omega') \\
 &= \int k_{\mathbf{Y}}(\mathbf{y}, \cdot) k_{\mathbf{A}}(\mathbf{a}, \cdot) d\mathbb{P}_{\mathbf{Y} \mid \mathbf{Z}=\mathbf{z}_\omega} \mathbb{P}_{\mathbf{A} \mid \mathbf{Z}=\mathbf{z}_\omega} && \text{(by definition of } k) \\
 &= \int k_{\mathbf{Y}}(\mathbf{y}, \cdot) d\mathbb{P}_{\mathbf{Y} \mid \mathbf{Z}=\mathbf{z}_\omega} \otimes \int k_{\mathbf{A}}(\mathbf{a}, \cdot) d\mathbb{P}_{\mathbf{A} \mid \mathbf{Z}=\mathbf{z}_\omega} && \text{(by Fubini's Theorem)} \\
 &= \mu_{\mathbf{Y} \mid \mathbf{Z}=\mathbf{z}_\omega} \otimes \mu_{\mathbf{A} \mid \mathbf{Z}=\mathbf{z}_\omega}. && \text{(by definition)}
 \end{aligned}$$

The claim follows. □

## C Conditional kernel mean embeddings and the HSCIC

The notion of conditional kernel mean embeddings has already been studied in the literature. We show that, under stronger assumptions, our definition is equivalent to the definition by [Park and Muandet \[2020\]](#).

<sup>3</sup>The tensor product kernel  $k$  is characteristic if the mapping  $\mathbb{P}_{\mathbf{Y}, \mathbf{A}} \mapsto \mathbb{E}[k(\cdot, \mathbf{y} \otimes \mathbf{a})]$  is injective. Here, the expected value is taken over the pair  $(\mathbf{y}, \mathbf{a})$ .

## C.1 Conditional kernel mean embeddings and conditional independence

We show that, under stronger assumptions, the HSCIC can be defined using the Bochner conditional expected value. The Bochner conditional expected value is defined as follows.

**Definition C.1.** Fix two random variables  $\mathbf{Y}$ ,  $\mathbf{Z}$  taking value in a Banach space  $\mathcal{H}$ , and denote with  $(\Omega, \mathcal{F}, \mathbb{P})$  their joint probability space. Then, the Bochner conditional expectation of  $\mathbf{Y}$  given  $\mathbf{Z}$  is any  $\mathcal{H}$ -valued random variable  $\mathbf{X}$  such that

$$\int_E \mathbf{Y} d\mathbb{P} = \int_E \mathbf{X} d\mathbb{P}$$

for all  $E \in \sigma(\mathbf{Z}) \subseteq \mathcal{F}$ , with  $\sigma(\mathbf{Z})$  the  $\sigma$ -algebra generated by  $\mathbf{Z}$ . We denote with  $\mathbb{E}[\mathbf{Y} | \mathbf{Z}]$  the Bochner expected value. Any random variable  $\mathbf{X}$  as above is a version of  $\mathbb{E}[\mathbf{Y} | \mathbf{Z}]$ .

The existence and almost sure uniqueness of the conditional expectation is shown in [Dinculeanu \[2000\]](#). Given a RKHS  $\mathcal{H}$  with kernel  $k$  over the support of  $\mathbf{Y}$ , [Park and Muandet \[2020\]](#) define the corresponding conditional kernel mean embedding as

$$\mu_{\mathbf{Y}|\mathbf{Z}} := \mathbb{E}[k(\cdot, \mathbf{y}) | \mathbf{Z}].$$

Note that, according to this definition,  $\mu_{\mathbf{Y}|\mathbf{Z}}$  is an  $\mathcal{H}$ -valued random variable, not a single point of  $\mathcal{H}$ . [Park and Muandet \[2020\]](#) use this notion to define the HSCIC as follows.

**Definition C.2** (The HSCIC according to [Park and Muandet \[2020\]](#)). Consider (sets of) random variables  $\mathbf{Y}$ ,  $\mathbf{A}$ ,  $\mathbf{Z}$ , and consider two RKHS  $\mathcal{H}_{\mathbf{Y}}$ ,  $\mathcal{H}_{\mathbf{A}}$  over the support of  $\mathbf{Y}$  and  $\mathbf{A}$  respectively. The HSCIC between  $\mathbf{Y}$  and  $\mathbf{A}$  given  $\mathbf{Z}$  is defined as the real-valued random variable

$$\omega \mapsto \|\mu_{\mathbf{Y}, \mathbf{A}|\mathbf{Z}}(\omega) - \mu_{\mathbf{Y}|\mathbf{Z}}(\omega) \otimes \mu_{\mathbf{A}|\mathbf{Z}}(\omega)\|,$$

for all samples  $\omega$  in the domain  $\Omega_{\mathbf{Z}}$  of  $\mathbf{Z}$ . Here,  $\|\cdot\|$  the metric induced by the inner product of the tensor product space  $\mathcal{H}_{\mathbf{Y}} \otimes \mathcal{H}_{\mathbf{Z}}$ .

We show that, under more restrictive assumptions, Definition C.2 can be used to promote conditional independence. To this end, we use the notion of a regular version.

**Definition C.3** (Regular Version, following Definition 2.4 by [Çinlar and ŞCinlar \[2011\]](#)). Consider two random variables  $\mathbf{Y}$ ,  $\mathbf{Z}$ , and consider the induced measurable spaces  $(\Omega_{\mathbf{Y}}, \mathcal{F}_{\mathbf{Y}})$  and  $(\Omega_{\mathbf{Z}}, \mathcal{F}_{\mathbf{Z}})$ . A regular version  $Q$  for  $\mathbb{P}_{\mathbf{Y}|\mathbf{Z}}$  is a mapping  $Q: \Omega_{\mathbf{Z}} \times \mathcal{F}_{\mathbf{Y}} \rightarrow [0, +\infty]: (\omega, \mathbf{y}) \mapsto Q_{\omega}(\mathbf{y})$  such that: (i) the map  $\omega \mapsto Q_{\omega}(\mathbf{x})$  is  $\mathcal{F}_{\mathbf{A}}$ -measurable for all  $\mathbf{y}$ ; (ii) the map  $\mathbf{y} \mapsto Q_{\omega}(\mathbf{y})$  is a measure on  $(\Omega_{\mathbf{Y}}, \mathcal{F}_{\mathbf{Y}})$  for all  $\omega$ ; (iii) the function  $Q_{\omega}(\mathbf{y})$  is a version for  $\mathbb{E}[\mathbb{1}_{\{\mathbf{Y}=\mathbf{y}\}} | \mathbf{Z}]$ .

The following theorem shows that the random variable as in Definition C.2 can be used to promote conditional independence.

**Theorem C.4** (Theorem 5.4 by [Park and Muandet \[2020\]](#)). *With the notation introduced above, suppose that the kernel  $k$  of the tensor product space  $\mathcal{H}_{\mathbf{X}} \otimes \mathcal{H}_{\mathbf{A}}$  is characteristic. Furthermore, suppose that  $\mathbb{P}_{\mathbf{Y}, \mathbf{A}|\mathbf{X}}$  admits a regular version. Then,  $\|\mu_{\mathbf{Y}, \mathbf{A}|\mathbf{Z}}(\omega) - \mu_{\mathbf{Y}|\mathbf{Z}}(\omega) \otimes \mu_{\mathbf{A}|\mathbf{Z}}(\omega)\| = 0$  almost surely if and only if  $\mathbf{Y} \perp\!\!\!\perp \mathbf{A} | \mathbf{Z}$ .*

Note that the assumption of the existence of a regular version is essential in Theorem C.4.

## C.2 Equivalence with our approach

The following theorem, shows that under the existence of a regular version, conditional kernel mean embeddings can be defined using the Bochner conditional expected value. To this end, we use the following theorem.

**Theorem C.5** (Following Proposition 2.5 by [Çinlar and δÇinlar \[2011\]](#)). *Following the notation introduced in Definition C.3, suppose that  $\mathbb{P}_{\mathbf{Y}|\mathbf{Z}}(\cdot | \mathbf{Z})$  admits a regular version  $Q_\omega(\mathbf{y})$ . Consider a kernel  $k$  over the support of  $\mathbf{Y}$ . Then, the mapping*

$$\omega \mapsto \int k(\cdot, \mathbf{y}) dQ_\omega(\mathbf{y})$$

*is a version of  $\mathbb{E}[k(\cdot, \mathbf{y}) | \mathbf{Z}]$ .*

As a consequence of Theorem C.5, we prove the following result.

**Lemma C.6.** *Fix two random variables  $\mathbf{Y}, \mathbf{Z}$ . Suppose that  $\mathbb{P}_{\mathbf{Y}|\mathbf{Z}}$  admits a regular version. Denote with  $\Omega_{\mathbf{Z}}$  the domain of  $\mathbf{Z}$ . Then, there exists a subset  $\Omega \subseteq \Omega_{\mathbf{Z}}$  that occurs almost surely, such that  $\mu_{\mathbf{Y}|\mathbf{Z}}(\omega) = \mu_{\mathbf{Y}|\mathbf{Z}=\mathbf{Z}(\omega)}$  for all  $\omega \in \Omega$ . Here,  $\mu_{\mathbf{Y}|\mathbf{Z}=\mathbf{z}(\omega)}$  is the embedding of conditional measures as in Section 2.*

*Proof.* Let  $Q_\omega(\mathbf{y})$  be a regular version of  $\mathbb{P}_{\mathbf{Y}|\mathbf{Z}}$ . Without loss of generality we may assume that it holds  $\mathbb{P}_{\mathbf{Y}|\mathbf{Z}}(\mathbf{y} | \{\mathbf{Z} = \mathbf{Z}(\omega)\}) = Q_\omega(\mathbf{y})$ . By Theorem C.5 there exists an event  $\Omega \subseteq \Omega_{\mathbf{Z}}$  that occurs almost surely such that

$$\mu_{\mathbf{Y}|\mathbf{Z}}(\omega) = \mathbb{E}[k(\mathbf{y}, \cdot) | \mathbf{Z}](\omega) = \int k(\mathbf{y}, \cdot) dQ_\omega(\mathbf{y}), \quad (7)$$

for all  $\omega \in \Omega$ . Then, for all  $\omega \in \Omega$  it holds

$$\begin{aligned} \mu_{\mathbf{Y}|\mathbf{Z}}(\omega) &= \int k(\mathbf{x}, \cdot) dQ_\omega(\mathbf{x}) && \text{(it follows from eq. (7))} \\ &= \int k(\mathbf{x}, \cdot) d\mathbb{P}_{\mathbf{X}|\mathbf{A}}(\mathbf{x} | \{\mathbf{A} = \mathbf{A}(\omega)\}) && (Q_\omega(\mathbf{y}) = \mathbb{P}_{\mathbf{Y}|\mathbf{Z}}(\mathbf{y} | \{\mathbf{Z} = \mathbf{Z}(\omega)\})) \\ &= \mu_{\mathbf{X}|\{\mathbf{A}=\mathbf{A}(\omega)\}}, && \text{(by definition as in Section 2)} \end{aligned}$$

as claimed. □

As a consequence of Lemma C.6, we can prove that the definition of the HSCIC by [Park and Muandet \[2020\]](#) is equivalent to ours. The following corollary holds.

**Corollary C.7.** *Consider (sets of) random variables  $\mathbf{Y}, \mathbf{A}, \mathbf{Z}$ , and consider two RKHS  $\mathcal{H}_{\mathbf{Y}}, \mathcal{H}_{\mathbf{A}}$  over the support of  $\mathbf{Y}$  and  $\mathbf{A}$  respectively. Suppose that  $\mathbb{P}_{\mathbf{Y},\mathbf{A}|\mathbf{Z}}(\cdot | \mathbf{Z})$  admits a regular version. Then, there exists a set  $\Omega \subseteq \Omega_{\mathbf{A}}$  that occurs almost surely, such that*

$$\|\mu_{\mathbf{X},\mathbf{A}|\mathbf{Z}}(\omega) - \mu_{\mathbf{X}|\mathbf{Z}}(\omega) \otimes \mu_{\mathbf{A}|\mathbf{Z}}(\omega)\| = (H_{\mathbf{Y},\mathbf{A}|\mathbf{Z}} \circ \mathbf{Z})(\omega).$$

Here,  $H_{\mathbf{Y},\mathbf{A}|\mathbf{Z}}$  is a real-valued deterministic function, defined as

$$H_{\mathbf{Y},\mathbf{A}|\mathbf{Z}}(\mathbf{z}) := \|\mu_{\mathbf{Y},\mathbf{A}|\mathbf{Z}=\mathbf{z}} - \mu_{\mathbf{Y}|\mathbf{Z}=\mathbf{z}} \otimes \mu_{\mathbf{A}|\mathbf{Z}=\mathbf{z}}\|,$$

and  $\|\cdot\|$  is the metric induced by the inner product of the tensor product space  $\mathcal{H}_{\mathbf{X}} \otimes \mathcal{H}_{\mathbf{A}}$ .

We remark that the assumption of the existence of a regular version is essential in Corollary C.7.

## D Conditional independence and the cross-covariance operator

In this section, we show that under additional assumptions, our definition of conditional KMEs is equivalent to the definition based on the cross-covariance operator, under more restrictive assumptions.

The definition of KMEs based on the cross-covariance operator requires the use of the following well-known result.

**Lemma D.1.** Fix two RKHS  $\mathcal{H}_{\mathbf{X}}$  and  $\mathcal{H}_{\mathbf{Z}}$ , and let  $\{\varphi_i\}_{i=1}^{\infty}$  and  $\{\psi_j\}_{j=1}^{\infty}$  be orthonormal bases of  $\mathcal{H}_{\mathbf{X}}$  and  $\mathcal{H}_{\mathbf{Z}}$  respectively. Denote with  $\text{HS}(\mathcal{H}_{\mathbf{X}}, \mathcal{H}_{\mathbf{Z}})$  the set of Hilbert-Schmidt operators between  $\mathcal{H}_{\mathbf{X}}$  and  $\mathcal{H}_{\mathbf{Z}}$ . There is an isometric isomorphism between the tensor product space  $\mathcal{H}_{\mathbf{X}} \otimes \mathcal{H}_{\mathbf{Z}}$  and  $\text{HS}(\mathcal{H}_{\mathbf{X}}, \mathcal{H}_{\mathbf{Z}})$ , given by the map

$$T: \sum_{i=1}^{\infty} \sum_{j=1}^{\infty} c_{i,j} \varphi_i \otimes \psi_j \mapsto \sum_{i=1}^{\infty} \sum_{j=1}^{\infty} c_{i,j} \langle \cdot, \varphi_i \rangle_{\mathcal{H}_{\mathbf{X}}} \psi_j.$$

For a proof of this result see i.e., [Park and Muandet \[2020\]](#). This lemma allows us to define the cross-covariance operator between two random variables, using the operator  $T$ .

**Definition D.2** (Cross-Covariance Operator). Consider two random variables  $\mathbf{X}$ ,  $\mathbf{Z}$ . Consider corresponding mean embeddings  $\mu_{\mathbf{X}, \mathbf{Z}}$ ,  $\mu_{\mathbf{X}}$  and  $\mu_{\mathbf{Z}}$ , as defined in Section 3. The cross-covariance operator is defined as  $\Sigma_{\mathbf{X}, \mathbf{Z}} := T(\mu_{\mathbf{X}, \mathbf{Z}} - \mu_{\mathbf{X}} \otimes \mu_{\mathbf{Z}})$ . Here,  $T$  is the isometric isomorphism as in Lemma D.1.

It is well-known that the cross-covariance operator can be decomposed into the covariance of the marginals and the correlation. That is, there exists a unique bounded operator  $\Lambda_{\mathbf{Y}, \mathbf{Z}}$  such that

$$\Sigma_{\mathbf{Y}, \mathbf{Z}} = \Sigma_{\mathbf{Y}, \mathbf{Y}}^{1/2} \circ \Lambda_{\mathbf{Y}, \mathbf{Z}} \circ \Sigma_{\mathbf{Z}, \mathbf{Z}}^{1/2}$$

Using this notation, we define the *normalized conditional cross-covariance operator*. Given three random variables  $\mathbf{Y}$ ,  $\mathbf{A}$ ,  $\mathbf{Z}$  and corresponding kernel mean embeddings, this operator is defined as

$$\Lambda_{\mathbf{Y}, \mathbf{A} | \mathbf{Z}} := \Lambda_{\mathbf{Y}, \mathbf{A}} - \Lambda_{\mathbf{Y}, \mathbf{Z}} \circ \Lambda_{\mathbf{Z}, \mathbf{A}}. \quad (8)$$

This operator was introduced by [Fukumizu et al. \[2007\]](#). The normalized conditional cross-covariance can be used to promote statistical independence, as shown in the following theorem.

**Theorem D.3** (Theorem 3 by [Fukumizu et al. \[2007\]](#)). Following the notation introduced above, define the random variable  $\tilde{\mathbf{A}} := (\mathbf{A}, \mathbf{Z})$ . Let  $\mathbb{P}_{\mathbf{Z}}$  be the distribution of the random variable  $\mathbf{Z}$ , and denote with  $L^2(\mathbb{P}_{\mathbf{Z}})$  the space of the square integrable functions with probability  $\mathbb{P}_{\mathbf{Z}}$ . Suppose that the tensor product kernel  $k_{\mathbf{Y}} \otimes k_{\mathbf{A}} \otimes k_{\mathbf{Z}}$  is characteristic. Furthermore, suppose that  $\mathcal{H}_{\mathbf{Z}} + \mathbb{R}$  is dense in  $L^2(\mathbb{P}_{\mathbf{Z}})$ . Then, it holds

$$\Lambda_{\mathbf{Y}, \tilde{\mathbf{A}} | \mathbf{Z}} = 0 \quad \text{if and only if} \quad \mathbf{Y} \perp\!\!\!\perp \mathbf{A} \mid \mathbf{X}.$$

Here,  $\Lambda_{\mathbf{Y}, \tilde{\mathbf{A}} | \mathbf{Z}}$  is an operator defined as in eq. (8).

By Theorem D.3, the operator  $\Lambda_{\mathbf{Y}, \tilde{\mathbf{A}} | \mathbf{Z}}$  can also be used to promote conditional independence. However, our method is more straightforward since it requires less assumptions. In fact, Theorem D.3 requires to embed the variable  $\mathbf{Z}$  in a RKHS. In contrast, our method only requires the embedding on the variables  $\mathbf{Y}$  and  $\mathbf{A}$ .

## E Random Fourier features

Random Fourier features is an approach to scaling up kernel methods for shift-invariant kernels [[Rahimi and Recht, 2007](#)]. Recall that a shift-invariant kernel is a kernel of the form  $k(\mathbf{z}, \mathbf{z}') = h_k(\mathbf{z} - \mathbf{z}')$ , with  $h_k$  a positive definite function.

Fourier features are defined via the following well-known theorem.

**Theorem E.1** (Bochner's Theorem). For every shift-invariant kernel of the form  $k(\mathbf{z}, \mathbf{z}') = h_k(\mathbf{z} - \mathbf{z}')$  with  $h_k(\mathbf{0}) = 1$ , there exists a probability density function  $\mathbb{P}_k(\boldsymbol{\eta})$  such that

$$k(\mathbf{z}, \mathbf{z}') = \int e^{-2\pi i \boldsymbol{\eta}^T (\mathbf{z} - \mathbf{z}')} d\mathbb{P}_k.$$

Since both the kernel  $k$  and the probability distribution  $\mathbb{P}_k$  are real-valued functions, the integrand in Theorem E.1 can be replaced by the function  $\cos \boldsymbol{\eta}^T(\mathbf{z} - \mathbf{z}')$ , and we obtain the following formula

$$k(\mathbf{z}, \mathbf{z}') = \int \cos \boldsymbol{\eta}^T(\mathbf{z} - \mathbf{z}') d\mathbb{P}_k = \mathbb{E} [\cos \boldsymbol{\eta}^T(\mathbf{z} - \mathbf{z}')], \quad (9)$$

where the expected value is taken with respect to the distribution  $\mathbb{P}_k(\boldsymbol{\eta})$ . This equation allows to approximate the kernel  $k(\mathbf{z}, \mathbf{z}')$ , via the empirical mean of points  $\boldsymbol{\eta}_1, \dots, \boldsymbol{\eta}_l$  sampled independently according to  $\mathbb{P}_k$ . In fact, it is possible to prove exponentially fast convergence of an empirical estimate for  $\mathbb{E} [\cos \boldsymbol{\eta}^T(\mathbf{z} - \mathbf{z}')]$ , as shown in the following theorem.

**Theorem E.2** (Uniform Convergence of Fourier Features, Claim 1 by [Rahimi and Recht \[2007\]](#)). *Following the notation introduced above, fix any compact subset  $\Omega$  in the domain of  $k$ , and consider points  $\boldsymbol{\eta}_1, \dots, \boldsymbol{\eta}_l$  sampled independent according to the distribution  $\mathbb{P}_k$ . Define the function*

$$\hat{k}(\mathbf{z}, \mathbf{z}') := \frac{1}{l} \sum_{j=1}^l \cos \boldsymbol{\eta}_j^T(\mathbf{z} - \mathbf{z}'),$$

for all  $(\mathbf{z}, \mathbf{z}') \in \Omega$ . Then, it holds

$$\mathbb{P} \left( \sup_{\mathbf{z}, \mathbf{z}'} |\hat{k}(\mathbf{z}, \mathbf{z}') - k(\mathbf{z}, \mathbf{z}')| \geq \varepsilon \right) \leq 2^8 \sigma_k \frac{\text{diam}(\Omega)}{\varepsilon} \exp \left\{ -\frac{\varepsilon^2 l}{4(d+1)} \right\}.$$

Here  $\sigma_k^2$  is the second moment of the Fourier transform of the kernel  $k$ , and  $d$  is the dimension of the arrays  $\mathbf{z}$  and  $\mathbf{z}'$ .

By Theorem E.2, the estimate kernel  $\hat{k}$  is a good approximation of the true kernel  $k$  on the set  $\Omega$ .

Similarly, we can approximate the Kernel matrix using Random Fourier features. Following the notation introduced above, define the function

$$\zeta_{k,l}(\mathbf{z}) := \frac{1}{\sqrt{l}} [\cos \boldsymbol{\eta}_1^T \mathbf{z}, \dots, \cos \boldsymbol{\eta}_l^T \mathbf{z}] \quad (10)$$

with  $\boldsymbol{\eta}_1, \dots, \boldsymbol{\eta}_l$  sampled independent according to the distribution  $\mathbb{P}_k$ .

We can approximate the Kernel matrix using the functions defined as in eq. (10). Consider  $n$  samples  $\mathbf{z}_1, \dots, \mathbf{z}_n$ , and denote with  $Z$  the  $n \times l$  matrix whose  $i$ -th row is given by  $\zeta_{k,l}(\mathbf{z}_i)$ . Similarly, denote with  $Z^*$  the  $l \times n$  matrix whose  $i$ -th column is given by  $\zeta_{k,l}^*(\mathbf{z}_i)$ . Then, we can approximate the kernel matrix as  $\hat{K}_{\mathbf{Z}} \approx ZZ^*$ .

We can also use this approximation to compute the kernel ridge regression parameters as in Section 3 using the formula  $\hat{w}_{\mathbf{Y}|\mathbf{Z}}(\cdot) \approx (ZZ^* - n\lambda I)^{-1} [k_{\mathbf{Z}}(\cdot, \mathbf{z}_1), \dots, k_{\mathbf{Z}}(\cdot, \mathbf{z}_n)]^T$ . [Avron et al. \[2017\]](#) argue that the approximate kernel ridge regression, as defined above, is an accurate estimate of the true distribution. Their argument is based on proving that the matrix  $ZZ^* - n\lambda I$  is a *good approximation* of  $\hat{K}_{\mathbf{Z}} - n\lambda I$ . The notion of good approximation is clarified by the following definition.

**Definition E.3.** Fix two Hermitian matrices  $A$  and  $B$  of the same size. We say that a matrix  $A$  is a  $\gamma$ -spectral approximation of another matrix  $B$ , if it holds  $(1 - \gamma)B \preceq A \preceq (1 + \gamma)B$ . Here, the  $\preceq$  symbol means that  $A - (1 - \gamma)B$  is positive semi-definite, and that  $(1 + \gamma)B - A$  is positive semi-definite.

[Avron et al. \[2017\]](#) prove that  $ZZ^* - n\lambda I$  is a  $\gamma$ -approximation of  $\hat{K}_{\mathbf{Z}} - n\lambda I$ , if the number of samples  $\boldsymbol{\eta}_1, \dots, \boldsymbol{\eta}_l$  is sufficiently large.



**Theorem E.4** (Theorem 7 by Avron et al. [2017]). Fix a constant  $\gamma \leq 1/2$ . Consider  $n$  samples  $\mathbf{z}_1, \dots, \mathbf{z}_n$ , and denote with  $\hat{K}_{\mathbf{Z}}$  the corresponding kernel matrix. Suppose that it holds  $\|\hat{K}_{\mathbf{Z}}\|_2 \geq n\lambda$  for a constant  $\lambda > 0$ . Fix  $\boldsymbol{\eta}_1, \dots, \boldsymbol{\eta}_l$  samples with

$$l \geq \frac{8}{3\gamma^2\lambda} \ln \frac{16 \operatorname{tr}_\lambda(\hat{K}_{\mathbf{Z}})}{\gamma}$$

Then, the matrix  $ZZ^* - n\lambda I$  is a  $\gamma$ -approximation of  $\hat{K}_{\mathbf{Z}} - n\lambda I$  with probability at least  $1 - \gamma$ , for all  $\gamma \in (0, 1)$ . Here,  $\operatorname{tr}_\lambda(\hat{K}_{\mathbf{Z}})$  is defined as the trace of the matrix  $\hat{K}_{\mathbf{Z}}(\hat{K}_{\mathbf{Z}} + n\lambda I)^{-1}$ .

We conclude this section by illustrating the use of random Fourier features to approximate a simple Gaussian kernel. Suppose that we are given a kernel of the form

$$k(\mathbf{z}, \mathbf{z}') := \exp \left\{ -\frac{1}{2} \sigma \|\mathbf{z} - \mathbf{z}'\|_2^2 \right\}.$$

Then,  $k(\mathbf{z}, \mathbf{z}')$  can be estimated as in Theorem E.2, with  $\boldsymbol{\eta}_1, \dots, \boldsymbol{\eta}_l \sim \mathcal{N}(0, \Sigma)$ , with  $\Sigma := \sigma^{-1}I$ , with  $I$  the identity matrix. The functions  $\zeta_{k,l}(\mathbf{z})$  can be defined accordingly.

## F Experiment settings

Additional information about the experiments is now provided. The interested reader may refer to the source code provided in the supplementary material. In all cases, the experiments were performed on an Apple M1 Pro. No external GPU sources were used for the experimental setup.

### F.1 Datasets for model performance with the use of the HSCIC

The first set of synthetic experiments involves three different dataset simulations. The data-generating mechanism corresponding to the results in Figure 4 is the following:

$$\begin{aligned} \mathbf{Z} &\sim \mathcal{N}(0, 1) & \mathbf{A} &= \mathbf{Z}^2 + \varepsilon_{\mathbf{A}} \\ \mathbf{X} &= \exp \left\{ -\frac{1}{5} \mathbf{A} \right\} \mathbf{A} + \sin(2\mathbf{Z}) + \frac{1}{5} \varepsilon_{\mathbf{X}} \\ \mathbf{Y} &= \frac{1}{2} \exp \{ -\mathbf{XZ} \} \cdot \sin(2\mathbf{XZ}) + 5\mathbf{A} + \frac{1}{5} \varepsilon_{\mathbf{Y}}, \end{aligned}$$

where  $\varepsilon_{\mathbf{A}} \sim \mathcal{N}(0, 1)$  and  $\varepsilon_{\mathbf{Y}}, \varepsilon_{\mathbf{X}} \stackrel{i.i.d.}{\sim} \mathcal{N}(0, 0.1)$ .

### F.2 Datasets for comparison with baselines

The simulation procedure for the Scenario 1 and Scenario 2 in Table 1 respectively are the following. Scenario 1:

$$\begin{aligned} \mathbf{Z} &\sim \mathcal{N}(0, 1) & \mathbf{A} &= \mathbf{Z}^2 + \varepsilon_{\mathbf{A}} \\ \mathbf{X} &= \frac{1}{2} \mathbf{A} * \varepsilon_{\mathbf{X}} + 2\mathbf{Z} \\ \mathbf{Y} &= \frac{1}{2} \exp \{ -\mathbf{XZ} \} \cdot \sin(2\mathbf{XZ}) + 5\mathbf{A} + \frac{1}{5} \varepsilon_{\mathbf{Y}}, \end{aligned}$$

where  $\varepsilon_{\mathbf{A}}, \varepsilon_{\mathbf{X}} \stackrel{i.i.d.}{\sim} \mathcal{N}(0, 1)$  and  $\varepsilon_{\mathbf{Y}} \stackrel{i.i.d.}{\sim} \mathcal{N}(0, 0.1)$ . Scenario 2:

$$\begin{aligned}\mathbf{Z} &\sim \mathcal{N}(0, 1) & \mathbf{A} &= \mathbf{Z}^2 + \varepsilon_{\mathbf{A}} \\ \mathbf{X} &= \frac{1}{5}\mathbf{A} * \varepsilon_{\mathbf{X}} + 2 \exp\left\{-\frac{1}{2}\mathbf{Z}^2\right\} \\ \mathbf{Y} &= \exp\{-\mathbf{Z}^2\} + \mathbf{A}\mathbf{X} + \frac{1}{5}\varepsilon_{\mathbf{Y}},\end{aligned}$$

where  $\varepsilon_{\mathbf{A}}, \varepsilon_{\mathbf{X}} \stackrel{i.i.d.}{\sim} \mathcal{N}(0, 1)$  and  $\varepsilon_{\mathbf{Y}} \stackrel{i.i.d.}{\sim} \mathcal{N}(0, 0.1)$ .

In the first experiment, Figure 4 shows the results of feed-forward neural networks consisting of 8 hidden layers with 20 nodes each, connected with a rectified linear activation function (ReLU) and a linear final layer. Mini-batch size of 256 and the Adam optimizer with a learning rate of  $10^{-3}$  for 100 epochs were used.

Analysing the results in Table 1, the same hyperparameters as in the previous setting. Here, both Scenario 1 and Scenario 2 were considered. The results shown in Figure 4 and Table 1 are the average and standard deviation resulting from respectively 10 and 4 random seeds runs.

### F.3 Datasets for multi-dimensional variables experiments

The data-generating mechanisms for the multi-dimensional settings of Tables 2 and 3 are now shown. Analysing the results in Table 2, given  $\dim\mathbf{A} = D_1 \geq 2$ , the datasets were generated from:

$$\begin{aligned}\mathbf{Z} &\sim \mathcal{N}(0, 1) & \mathbf{A}_i &= \mathbf{Z}^2 + \varepsilon_{\mathbf{A}}^i \quad \text{for } i \in \{1, D_1\} \\ \mathbf{X} &= \exp\left\{-\frac{1}{2}\mathbf{A}_1\right\} + \sum_{i=1}^{D_1} \mathbf{A}_i \cdot \sin(\mathbf{Z}) + 0.1 \cdot \varepsilon_{\mathbf{X}} \\ \mathbf{Y} &= \exp\left\{-\frac{1}{2}\mathbf{A}_2\right\} \cdot \sum_{i=1}^{D_1} \mathbf{A}_i + \mathbf{X}\mathbf{Z} + 0.1 \cdot \varepsilon_{\mathbf{Y}},\end{aligned}$$

where  $\varepsilon_{\mathbf{X}}, \varepsilon_{\mathbf{Y}} \stackrel{i.i.d.}{\sim} \mathcal{N}(0, 0.1)$  and  $\varepsilon_{\mathbf{A}}^1, \dots, \varepsilon_{\mathbf{A}}^{D_1} \stackrel{i.i.d.}{\sim} \mathcal{N}(0, 1)$ . In this setting, the mini-batch size chosen is 64 and the same hyperparameters are used as in the previous setting. The neural network architecture is trained for 70 epochs.

In Table 3 the following data-generating process is used:

$$\begin{aligned}\mathbf{Z}_1, \mathbf{Z}_2, \dots, \mathbf{Z}_{D_2} &\stackrel{i.i.d.}{\sim} \mathcal{N}(0, 1) & \mathbf{A} &= \sum_{i=1}^{D_2} \mathbf{Z}_i^2 + \varepsilon_{\mathbf{A}} \\ \mathbf{X} &= \exp\left\{-\frac{1}{2}\mathbf{A}\right\} + \sin\left(\sum_{i=1}^{D_2} \mathbf{Z}_i\right) \cdot \mathbf{A} + 0.1 \cdot \varepsilon_{\mathbf{X}} \\ \mathbf{Y} &= \exp\left\{-\frac{1}{2}\mathbf{A}\right\} \cdot \mathbf{A} + \sum_{i=1}^{D_2} \mathbf{Z}_i + \mathbf{A} + \mathbf{X}\mathbf{Z}_1 + 0.1 \cdot \varepsilon_{\mathbf{Y}},\end{aligned}$$

with  $\dim\mathbf{Z} = D_2 \geq 2$  and  $\varepsilon_{\mathbf{A}} \sim \mathcal{N}(0, 1)$ ,  $\varepsilon_{\mathbf{X}}, \varepsilon_{\mathbf{Y}} \stackrel{i.i.d.}{\sim} \mathcal{N}(0, 0.1)$ . Here, we used mini-batch size of 32, a learning rate of  $10^{-4}$  and a number of epochs of 500.

Table 4: **Results of MSE, HSCIC, VCF (all times  $10^5$  for readability) on synthetic data** with bi-dimensional  $\mathbf{A}$  and  $\mathbf{Z}$ . Here  $\dim\mathbf{Z} = 2, \dim\mathbf{A} = 2, \dim\mathbf{X} = 1, \dim\mathbf{Y} = 1$ .

	MSE	HSCIC	VCF
$\gamma = 0$	$0.315 \pm 0.055$	$13854.1 \pm 8.47$	$24.6 \pm 1.17$
$\gamma = \frac{1}{2}$	$0.336 \pm 0.0525$	$13854.0 \pm 8.46$	$22.9 \pm 0.69$
$\gamma = 1$	$0.393 \pm 0.162$	$13853.9 \pm 8.46$	$20.4 \pm 2.02$

The results in Tables 2 and 3 are the average obtained from three random seeds runs on the same data-split.

We tested the method on a further setting, consisting of bi-dimensional  $\mathbf{Z}$  and  $\mathbf{A}$  ( $\dim\mathbf{A} = 2, \dim\mathbf{Z} = 2$ ). Specifically, we have  $\mathbf{Z} = \{\mathbf{Z}_1, \mathbf{Z}_2\}$  and  $\mathbf{A} = \{\mathbf{A}_1, \mathbf{A}_2\}$ . The data-generating mechanism is the following:

$$\mathbf{Z}_1 \sim \mathcal{N}(0, 1) \quad \mathbf{Z}_2 \sim \mathcal{N}(3, 0.1) \quad \mathbf{A}_1 = \mathbf{Z}_1^2 + \varepsilon_{\mathbf{A}_1} \quad \mathbf{A}_2 = \exp\{-0.1 \cdot (\mathbf{Z}_1 + \mathbf{Z}_2)\} + \varepsilon_{\mathbf{A}_2}$$

$$\mathbf{X} = \exp\left\{-\frac{1}{2}\mathbf{A}\right\} \cdot \sin(2 \cdot \mathbf{A}_1) + (\mathbf{Z}_1 + \mathbf{Z}_2) \cdot (\mathbf{A}_1 + \mathbf{A}_2) + 0.1 \cdot \varepsilon_{\mathbf{X}}$$

$$\mathbf{Y} = \exp\left\{-\frac{1}{2}\mathbf{A}_1^2\right\} \cdot \sin(2 \cdot \mathbf{A}_2^2) + \mathbf{X} \cdot (\mathbf{Z}_1 + \mathbf{Z}_2) + 5 \cdot \mathbf{A}_1 \cdot \mathbf{A}_2 + 0.1 \cdot \varepsilon_{\mathbf{Y}},$$

where  $\varepsilon_{\mathbf{Y}}, \varepsilon_{\mathbf{X}}, \varepsilon_{\mathbf{A}_1}, \varepsilon_{\mathbf{A}_2} \stackrel{i.i.d.}{\sim} \mathcal{N}(0, 0.1)$ . In Table 4, the trade-off between accuracy and counterfactually invariant predictions is once again shown, implying that the proposed method can also be applied in settings where both  $\mathbf{Z}$  and  $\mathbf{A}$  are not unidimensional. In Table 4 the average and standard deviation of the results from four runs with random seed and re-sampled data are presented.

#### F.4 High-dimensional image dataset

The simulation procedure for the results shown in Section 5.2 is the following.

$$\begin{aligned} \text{shape} &\sim \mathbb{P}(\text{shape}) \\ \text{y-pos} &\sim \mathbb{P}(\text{y-pos}) \\ \text{color} &\sim \mathbb{P}(\text{color}) \\ \text{orientation} &\sim \mathbb{P}(\text{orientation}) \\ \text{x-pos} &= \text{round}(x), \text{ where } x \sim \mathcal{N}(\text{shape} + \text{y-pos}, 1) \\ \text{scale} &= \text{round}\left(\left(\frac{\text{x-pos}}{24} + \frac{\text{y-pos}}{24}\right) \cdot \text{shape} + \epsilon_S\right) \\ \mathbf{Y} &= e^{\text{shape}} \cdot \text{x-pos} + \text{scale}^2 \cdot \sin(\text{y-pos}) + \epsilon_Y, \end{aligned}$$

where  $\epsilon_S \sim \mathcal{N}(0, 1)$  and  $\epsilon_Y \sim \mathcal{N}(0, 0.01)$ . The data has been generated via a matching procedure on the original dSprites dataset.

In Table 5, the hyperparameters of the layers of the convolutional neural network are presented. Each of the convolutional groups also has a ReLU activation function and a dropout layer. Two MLP architectures have been used. The former takes as input the observed tabular features. It is composed by two hidden layers of 16 and 8 nodes respectively, connected with ReLU activation functions and dropout layers. The latter takes as input the concatenated outcomes of the CNN and the other MLP. It consists of three hidden layers of 8, 8 and 16 nodes, respectively. Figure 5 presents the averaged results of four random seeds runs with new sampled data.

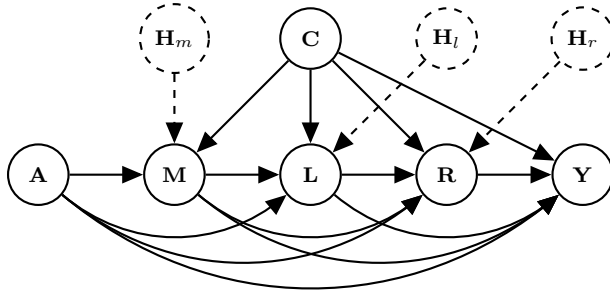


Figure 8: **Assumed causal graph for the Adult dataset**, as in [Chiappa and Pacchiano \[2021\]](#). The variables  $\mathbf{H}_m$ ,  $\mathbf{H}_l$ ,  $\mathbf{H}_r$  are unobserved, and jointly trained with the predictor  $\hat{\mathbf{Y}}$ .

### F.5 Fairness with continuous protected attributes

The pre-processing of the UCI Adult dataset was based upon the work of [\[Chiappa and Pacchiano, 2021\]](#). Referring to the causal graph in Figure 8, a variational autoencoder [\[Kingma and Welling, 2014\]](#) was trained for each of the unobserved variables  $\mathbf{H}_m$ ,  $\mathbf{H}_l$  and  $\mathbf{H}_r$ . The prior distribution of these latent variables is assumed to be standard Gaussian. The posterior distributions  $\mathbb{P}(\mathbf{H}_m|V)$ ,  $\mathbb{P}(\mathbf{H}_r|V)$ ,  $\mathbb{P}(\mathbf{H}_l|V)$  are modelled as 10-dimensional Gaussian distributions, whose means and variances are the outputs of the encoder.

The encoder architecture consists of a hidden layer of 20 hidden nodes with hyperbolic tangent activation functions, followed by a linear layer. The decoders have two linear layers with hyperbolic tangent activation function. The training loss of the variational autoencoder consists of a reconstruction term (Mean-Squared Error for continuous variables and Cross-Entropy Loss for binary ones) and the Kullback–Leibler divergence between the posterior and the prior distribution of the latent variables. For training, we used the Adam optimizer with learning rate of  $10^{-2}$ , 30 epochs, mini-batch size 128.

The predictor  $\hat{\mathbf{Y}}$  is the output of a feed-forward neural network consisting of a hidden layer with hyperbolic tangent activation function and a linear final layer. In the training we used the Adam optimizer with learning rate  $10^{-3}$ , mini-batch size 128, and trained for 100 epochs. The choice of the network architecture is based on the work of [\[Chiappa and Pacchiano, 2021\]](#).

The estimation of counterfactual outcomes is based on a Monte-Carlo approach. Given a data point, 500 values of the unobserved variables are sampled from the estimated posterior distribution. Given an interventional value for  $A$ , a counterfactual outcome is estimated for each of the sampled unobserved values. The final counterfactual outcome is estimated as the

Table 5: **Architecture of the convolutional neural network** used for the image dataset, as described in Appendix F.4.

layer	# filters	kernel size	stride size	padding size
convolution	16	5	2	2
max pooling	1	3	2	0
convolution	64	5	1	2
max pooling	1	1	2	0
convolution	64	5	1	2
max pooling	1	2	1	0
convolution	16	5	1	3
max pooling	1	2	2	0

average of these counterfactual predictions. In this experiment setting, we have  $k = 100$  and  $d = 1000$ .

In the causal graph presented in Figure 8,  $\mathbf{A}$  includes the variables age and gender,  $\mathbf{C}$  includes nationality and race,  $\mathbf{M}$  marital status,  $\mathbf{L}$  level of education,  $\mathbf{R}$  the set of working class, occupation, and hours per week and  $\mathbf{Y}$  the income class. Compared to [Chiappa and Pacchiano, 2021], we include the race variable in the dataset as part of the baseline features  $\mathbf{C}$ . The loss function is the same as Equation 2 but Binary Cross-Entropy loss is used instead of Mean-Squared Error loss:

$$\mathcal{L}_{\text{TOTAL}}(\hat{\mathbf{Y}}) = \mathcal{L}_{\text{BCE}}(\hat{\mathbf{Y}}) + \gamma \cdot \text{HSCIC} \left( \hat{\mathbf{Y}}, \{\text{Age, Gender}\} \middle| \mathbf{Z} \right), \quad (11)$$

where the set  $\mathbf{Z}$  blocks all the non-directed paths from  $\mathbf{W} \cup \mathbf{A}$ . In this example we have  $\mathbf{W} = \{\mathbf{C} \cup \mathbf{M} \cup \mathbf{L} \cup \mathbf{R}\}$ . The results in Figure 6 (center, right) refer to one run with conditioning set  $\mathbf{Z} = \{\text{Race, Nationality}\}$ . The results in Table 6 (right) are the average and standard deviation of four random seeds.